6-2010

Hydrodynamic Fin Function of Brief Squid, Lolliguncula Brevis

William J. Stewart

Ian K. Bartol
Old Dominion University, ibartol@odu.edu

Paul S. Krueger

Repository Citation

Stewart, William J.; Bartol, Ian K.; and Krueger, Paul S., "Hydrodynamic Fin Function of Brief Squid, Lolliguncula Brevis" (2010). *Biological Sciences Faculty Publications*. 195.
https://digitalcommons.odu.edu/biology_fac_pubs/195

Original Publication Citation

Stewart, W. J., Bartol, I. K., & Krueger, P. S. (2010). Hydrodynamic fin function of brief squid, *Lolliguncula brevis*. *Journal of Experimental Biology, 213*(12), 2009-2024. doi:10.1242/jeb.039057

The Journal of Experimental Biology 213, 2009-2024

doi:10.1242/jeb.039057

Hydrodynamic fin function of brief squid, *Lolliguncula brevis*

William J. Stewart[1,*], Ian K. Bartol[2] and Paul S. Krueger[3]

[1]University of California-Irvine, Irvine, CA 92697, USA, [2]Old Dominion University, Norfolk, VA 23529, USA and [3]Southern Methodist University, Dallas, TX 75275, USA

*Author for correspondence (wstewart@uci.edu)

Accepted 4 March 2010

SUMMARY

Although the pulsed jet is often considered the foundation of a squid's locomotive system, the lateral fins also probably play an important role in swimming, potentially providing thrust, lift and dynamic stability as needed. Fin morphology and movement vary greatly among squid species, but the locomotive role of the fins is not well understood. To begin to elucidate the locomotive role of the fins in squids, fin hydrodynamics were studied in the brief squid *Lolliguncula brevis*, a species that exhibits a wide range of fin movements depending on swimming speed. Individual squid were trained to swim in both the arms-first and tail-first orientations against currents in a water tunnel seeded with light-reflective particles. Particle-laden water around the fins was illuminated with lasers and videotaped so that flow dynamics around the fins could be analyzed using digital particle image velocimetry (DPIV). Time-averaged forces generated by the fin were quantified from vorticity fields of the fin wake. During the low swimming speeds considered in this study [<2.5 dorsal mantle lengths (*DML*) per second], *L. brevis* exhibited four unique fin wake patterns, each with distinctive vortical structures: (1) fin mode I, in which one vortex is shed with each downstroke, generally occurring at low speeds; (2) fin mode II, an undulatory mode in which a continuous linked chain of vortices is produced; (3) fin mode III, in which one vortex is shed with each downstroke and upstroke, and; (4) fin mode IV, in which a discontinuous chain of linked double vortex structures is produced. All modes were detected during tail-first swimming but only fin modes II and III were observed during arms-first swimming. The fins produced horizontal and vertical forces of varying degrees depending on stroke phase, swimming speed, and swimming orientation. During tail-first swimming, the fins functioned primarily as stabilizers at low speeds before shifting to propulsors as speed increased, all while generating net lift. During arms-first swimming, the fins primarily provided lift with thrust production playing a reduced role. These results demonstrate the lateral fins are an integral component of the complex locomotive system of *L. brevis*, producing lift and thrust forces through different locomotive modes.

Key words: digital particle image velocimetry, fin, lift, locomotion, squid, thrust.

INTRODUCTION

Squid employ a complex locomotive approach involving two separate systems, the pulsed jet and movement of the lateral fins (Bartol et al., 2001b). However, many studies involving squid swimming performance have focused primarily on the jet while largely ignoring fin contributions to propulsion (Johnson et al., 1972; Anderson and DeMont, 2000; Anderson and Grosenbaugh, 2005; O'Dor, 1988), with other studies assuming the fins function only in stability and steering (O'Dor and Webber, 1991; Webber and O'Dor, 1986). As suggested by O'Dor (O'Dor, 1988), Hoar et al. (Hoar et al., 1994), Bartol et al. (Bartol et al., 2001b; Bartol et al., 2008) and Anderson and DeMont (Anderson and DeMont, 2005), the fins of squid may play important roles in lift and thrust production at various speeds. In fact, based on force balance predictions by Bartol et al. (Bartol et al., 2001b), the fins of shallow-water squids may produce more lift and thrust forces than the jet at certain speeds.

Both the morphometric form and function of fins vary across squid species (Hoar et al., 1994). Pelagic, fast moving ommastrephid squid have stout, triangular fins that flap during low speed cruising and extend outward at higher speeds, presumably to act as rudders (O'Dor and Webber, 1991; Webber and O'Dor, 1986). The small shape of the fins is important for drag reduction at higher swimming speeds but does not lend itself well to low-speed undulatory swimming. By contrast, the larger fins of coastal squid are used not only for maneuvering and stability, but also thrust production at low to moderate speeds (Anderson and Demont, 2005; Bartol et al., 2001b). Partly because of the increased drag acting on these larger fins, inshore myopsid squid often wrap the fins tightly around the mantle at high speeds (O'Dor, 1982; O'Dor, 1988). The absence of fin motion at these higher speeds is probably a product of support limitations of the fin's muscular hydrostat (Kier, 1989). Deep sea squids living at meso- and bathypelagic depths rely even more heavily on fin locomotion than shallow water species. Many deep-sea squid species have large fins that slowly undulate or flap to achieve relatively low swimming velocities, even during escape responses. These large fins presumably are responsible for the majority of locomotive forces, with the jet playing a reduced role (Vecchione et al., 2001; Vecchione et al., 2002).

Despite intriguing differences in fin form and function, very little is known about the locomotive role of fins in any squid. O'Dor (O'Dor, 1988), Hoar et al. (Hoar et al., 1994), Bartol et al. (Bartol et al., 2001b) and Anderson and DeMont (Anderson and DeMont, 2005) have all collected kinematic data that provide a valuable record of fin movements in various squid species (e.g. fin wave speed, fin amplitude, fin wave shape), and Bartol et al. (Bartol et al., 2001b), O'Dor (O'Dor, 1988) and Anderson and DeMont (Anderson and DeMont, 2005) made fin force predictions based largely on kinematic data. However, little qualitative or quantitative data of flows around the fins that can be used to understand force production have been collected to date.

A swimming or flying organism generates locomotive forces by transferring momentum into the fluid wake, which is often characterized by discrete vortices. The momentum associated with these vortices thus can be used to estimate locomotive forces (Peng et al., 2007). The technique of digital particle image velocimetry (DPIV) (Willert and Gharib, 1991) allows for the flow quantification and visualization of vortices around a swimming organism, and has been used in several studies to estimate the pectoral fin force contributions of fish (Drucker and Lauder, 1999; Drucker and Lauder, 2001; Drucker and Lauder, 2003). For this study, DPIV was used to measure flows and estimate force production associated with the fins of *Lolliguncula brevis*, to better understand locomotive fin function.

Brief squid, *Lolliguncula brevis*, are shallow water, coastal organisms with relatively large, rounded lateral fins. These euryhaline squid are highly maneuverable (Bartol et al., 2002) and presumably rely heavily on fins for locomotion (Hoar et al., 1994). Bartol et al. (Bartol et al., 2001b) extensively studied *L. brevis* kinematics and predicted that the fins actively produce lift and thrust, especially at low swimming speeds. Furthermore, *L. brevis* exhibits a range of fin movements, from undulations at low speeds to transitional undulatory flapping at intermediate speeds to more defined flapping at higher speeds (Bartol et al., 2001b). This heavy reliance on fin motion coupled with the versatility of fin movements afforded by the muscular hydrostatic system make *L. brevis* an excellent subject to study squid fin locomotion.

This study had three specific objectives: (1) to determine if the fins generate significant locomotive forces, (2) to describe any wake patterns produced by the fins, and (3) to document how lift and thrust production by the fins change with speed. Although squid employ a complex dual mode locomotive system involving both fins and a pulsed jet and this study focuses on only one component of this system, it provides the first quantitative data on fin flows around squids, which will help us better understand the complete locomotive strategy of squid. Fin function was investigated during both arms-first and tail-first swimming because squid swim in two different orientations. Although *Lolliguncula* does not have a pronounced anatomical tail like other squids, we use ‘tail-first swimming’ for convenience to describe a mode of swimming where the posterior portion of the mantle is at the leading edge.

MATERIALS AND METHODS

Animal maintenance

Adult specimens of *Lolliguncula brevis* Blainville (3.5–9 cm dorsal mantle length; *DML*) were captured by otter trawl within embayments near Wachapreague on the Eastern Shore of Virginia, USA. Trawls were conducted during August, September and October because *L. brevis* catch probabilities are highest within the Chesapeake Bay during this time (Bartol et al., 2002). Captured *L. brevis* were quickly and carefully transferred first to a bucket for ink release before being placed in a 114 liter, circular holding tank (Angler livewells, Aquatic Eco-Systems, Inc., Apopka, FL, USA) fitted with two portable battery-powered aerators (Model B-3, Marine Metal Products Co., Inc., Clearwater, FL, USA) for transport to the lab. A maximum of 12 individuals were kept in a single livewell to avoid stress from overcrowding.

In the lab, all individuals were housed in a 3-tank, 600 liter artificial seawater system filled with water maintained at temperatures and salinities equal to those of the capture sites (19–22°C; 30–35‰, respectively). The tanks were circular with moderate current flow to reduce wall abrasions and promote active swimming, as suggested by Hanlon et al. (Hanlon et al., 1983). Squid were fed a plentiful diet of live *Palaemonetes pugio* and *Fundulus* spp. and allowed to acclimatize for at least 24 h before experimentation. Given that the seawater system consists of three separate tanks, smaller individuals were kept separate from larger individuals to minimize intraspecific aggression. In total, 14 squid ranging from 3.5 to 6.2 cm *DML* were selected for this study.

Hydrodynamics

A 250 liter flume (Model 502{S}, Engineering Laboratory Design, Inc., Lake City, MN, USA) with a 15 cm×15 cm×43 cm working section was used for experimentation (Fig. 1). The flume was filled with aerated, artificial seawater of similar salinity and temperature to that present in the holding tanks. Only one squid was placed in the flume at a time for experimentation. Squid initially acclimated to the flume at speeds of 2–4 cm s^{-1} with low ambient light to minimize stress. After approximately 15–30 min of acclimation, when steady swimming was observed at the initial flume speed, hydrodynamic data were collected for several minutes depending on the squid’s behavior. The flow velocity of the flume was then slowly increased using 1 cm s^{-1} intervals, followed by another iteration of data collection once 5 min of steady swimming was observed. This procedure of flume speed elevation, acclimation and data collection was repeated until the squid could no longer keep pace with the flow. After experimentation, squid were over-anesthetized using a 10% solution of $MgCl_2$ (Messenger et al., 1985). Before preservation in formalin, the *DML* and mass of each squid were recorded. Fin area was calculated from digital images of

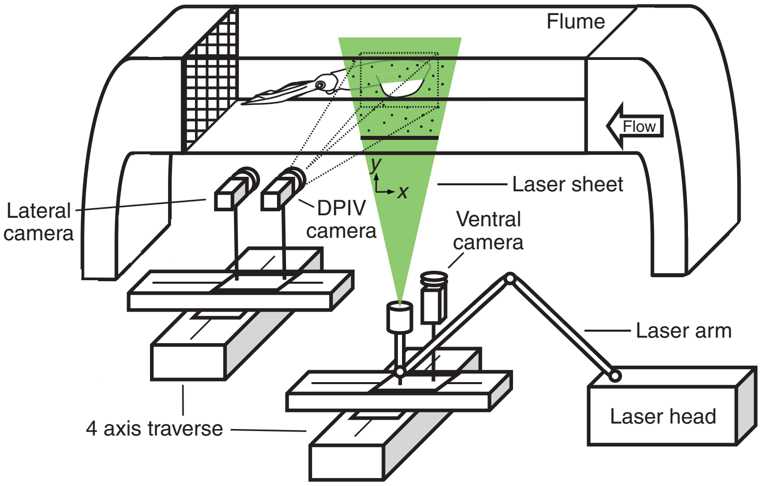

Fig. 1. Schematic representation of the experimental setup, illustrating the flume, laser, cameras, and 4-axis traverse.

preserved specimens using ImageJ image processing and analysis software (freeware: http://rsb.info.nih.gov/ij/).

A DPIV system was used to collect hydrodynamic data around one of the squid's lateral fins [i.e. the fin closest to the DPIV camera (see Fig. 1)] as it swam at the various flume speeds. Neutrally buoyant, silver-coated, hollow glass spheres (mean diameter=14 μm; Potters Industries, Inc., Malvern, PA, USA) were added to the flume for use as light-reflective particles. Two pulsed Nd:YAG lasers (wavelength=532 nm, power rating 350 mJ per pulse; LaBest Optronics Co. Ltd, Beijing, China), with an attached optical arm produced particle-illuminating light sheets, approximately 1 mm thick, from underneath the working section in the parasagittal (*x*–*y*) plane. The duration of each laser pulse was 7 ns and the time interval (Δt) between laser A and laser B firing was 1–4 ms. Each laser operated at 15 Hz, creating 15 laser pulse pairs per second. A CCD 'double shot' video camera (UP-1830CL, UNIQ Vision, Santa Clara, CA, USA) with a frame size of 1024×1024 pixels and a frame rate of 30 Hz was positioned to the side of the flume, perpendicular to the laser sheet, and was synchronized with the laser pulses to capture images of the illuminated particles. A CMOS video camera (Model 1M150-SA, DALSA, Waterloo, Ontario, Canada) was positioned underneath the working section to capture images from the ventral perspective. This camera was synchronized with the CCD camera and provided high resolution images (1024×1024 pixels) of the laser sheet position on the squid's body. A second, identical CMOS video camera (also synchronized with the CCD camera) was positioned directly beside the CCD video camera to provide an expanded lateral field of view of the mantle and fins (Fig. 1).

Synchronization of the cameras and laser pulses was achieved using an in-house timing program and PCI-6602 counter/timing card (National Instruments, Inc., Austin, TX, USA), which delivered a 5.0 V TTL triggering signal to the three video cameras and a pulse generator (Model 565, Berkeley Nucleonics Corp., San Rafael, CA, USA). The pulse generator locked onto the TTL signal and controlled the firing of the two lasers. Each video camera sent images to a separate CL-160 capture card (IO industries, Inc., London, Ontario, Canada), each of which provided direct data transfer to hard disk.

All cameras and the optical laser arm were mounted on a four-axis traverse system (Techno-Isel, New Hyde Park, NY, USA; Fig. 1). Using a joystick, a PCI-7344 motion controller board (National Instruments Inc., Austin, TX, USA), and a LabVIEW VI custom program (National Instruments, Inc., Austin, TX, USA), the three cameras and laser arm were moved simultaneously along the traverse to follow the target squid to different areas of the water tunnel. To avoid inaccurate flow measurements, data were only collected when the cameras and laser arm were not in motion. The traverse system was important because it allowed the laser sheet to be moved to desirable fin locations on the actively swimming squid.

DPIV data sequences ranging in length from approximately 10 to 200 image pairs were collected for all squid at various speeds. Only sequences in which the squid exhibited steady swimming while maintaining a relatively constant vertical position in the working section were considered for analysis. For those sequences where the squid did not perfectly match the free stream flow (tunnel speed), swimming velocity was calculated according to net horizontal displacement during each jet pulse. The laser sheets were positioned close to the terminal end of the squid's lateral fin as it translated through a stroke (Fig. 2). In total, 24 speeds of tail-first swimming and 14 speeds of arms-first swimming were used in the hydrodynamic analysis (each speed consisted of one to four image sequences; each image sequence consisted of two to five sequential fin stroke cycles).

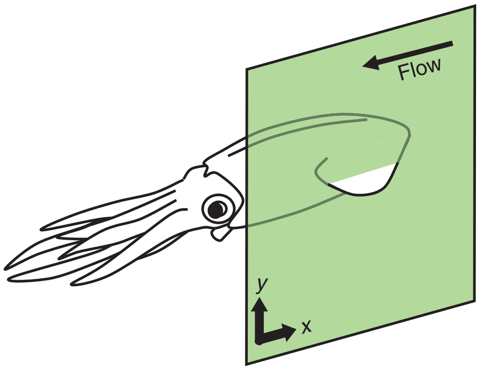

Fig. 2. Schematic diagram illustrating the laser sheet (wavelength=532 nm, thickness=1–2 mm), oriented vertically in the *x*–*y* plane, projecting through a squid's lateral fin while swimming in the tail-first orientation.

For analysis of the DPIV data, each image was divided into a matrix of 32×32 pixel interrogation windows with a 16 pixel offset (50% overlap) for cross-correlation analysis which yielded a 66×66 matrix of vectors. The remaining procedure for DPIV image analysis used in the present study was identical to that described in other studies (see Bartol et al., 2008; Bartol et al., 2009a; Bartol et al., 2009b), and thus we refer the reader to these studies for detailed descriptions of the protocols. As in previous locomotive studies involving fish (e.g. Drucker and Lauder, 1999; Müller et al., 1997; Müller et al., 2000; Tytell, 2004), time-averaged forces produced by the fin were estimated using DPIV data. Matlab utilities developed in-house were used to calculate hydrodynamic impulse and kinetic energy of vortices shed into the fin wake. Axisymmetry about the midline of shed vortex pairs was assumed in all calculations (i.e. vortex pairs were assumed to be circular vortex rings).

When vortices shed from sequential fin strokes were sufficiently spaced to consider the vortices 'isolated' (vortex spacing>two vortex diameters), hydrodynamic quantities were determined for each wake vortex (i.e. vortex ring) as follows. First, the location of the angled centerline of the vortex ring was determined based on the best fit of the velocity and vorticity data for the central jet of the vortex ring. The angle of the centerline (orientation of the central jet), was used to determine the vortex ring angle (Fig. 3A). Vortex ring angles were assigned values from 0 to ±180 deg depending on orientation relative to free-stream flow, with negative and positive values being assigned to angles above and below the free-stream axis, respectively. Second, using the angled centerline as the r=0 axis, jet impulse (magnitude) and kinetic energy were computed using the equations:

$$I / \rho = \pi \int_{\text{vortex}} \omega_\theta r^2 \,\mathrm{d}r\,\mathrm{d}x \qquad (1)$$

$$E / \rho = \pi \int_{\text{vortex}} \omega_\theta \psi \,\mathrm{d}r\,\mathrm{d}x \,, \qquad (2)$$

where I is magnitude of the hydrodynamic impulse, ω_θ is the azimuthal component of vorticity, r is the radial coordinate relative to the jet centerline, E is kinetic energy, ψ is the Stokes stream function, and ρ is fluid density. The area integrals were computed using a two-dimensional (2-D) version of the trapezoidal rule.

Time-averaged force contributions were determined separately for fin upstrokes and downstrokes at a particular swimming speed

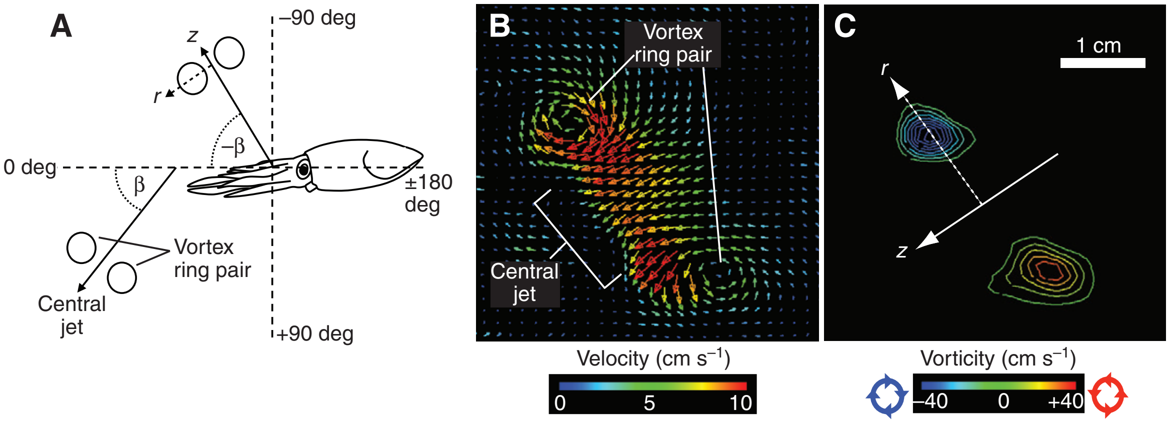

Fig. 3. (A) Schematic diagram illustrating two vortex rings generated by the fins for a squid (*Lolliguncula brevis*) swimming in the tail-first orientation. *z* represents the centerline of each vortex, β denotes the central jet angle, and *r* represents the radial coordinate relative to the jet centerline. The horizontal dashed line represents the axis parallel to free-stream flow (0 deg) and the vertical dashed line corresponds to the axis orthogonal to free-stream flow (–90/+90 deg). Any vortex angled above the horizontal 0 deg was assigned a negative β whereas a vortex angled below 0 deg was assigned a positive β. (B,C) The velocity vector field and corresponding vorticity contour field, respectively, of a typical vortex shed into the wake by a fin downstroke of *Lolliguncula brevis.* The squid fin lies dorsal to the field of view. Color scales: (B) red and blue vectors correspond to high and low velocities, respectively; (C) red regions represent counter-clockwise rotating fluid while blue regions represent clockwise rotating fluid.

using the results of Eqn 1. First, the impulse of a single downstroke was measured by calculating the average impulse of a shed vortex over two to four sequential frames. The impulse values of two to five sequential downstrokes were then averaged to determine the entire sequence's mean downstroke impulse. To calculate the time-averaged downstroke force, $\bar{F}_\mathrm{D}$, for a particular swimming sequence, the mean downstroke impulse of the sequence was divided by the average downstroke period. This time-averaged force, $\bar{F}_\mathrm{D}$, was then geometrically separated into horizontal thrust, $\bar{F}_\mathrm{T,D}$, and vertical lift, $\bar{F}_\mathrm{L,D}$, based on the mean vortex ring angle β (Fig. 3A). For simplicity, the use of the term 'lift' in this study refers to vertically oriented forces in the x–y plane, which should be a good approximation to the actual lift force as the free-stream flow in the water tunnel was horizontal and only sequences where the squid held vertical and horizontal station well were included in the study. This force calculation procedure was repeated for all upstrokes for each sequence. To account for any intraspecific variations in force production among squid of different body sizes, time-averaged forces were normalized according to fin area and expressed as $\mathrm{mN\,cm^{-2}}$. All swimming speeds were normalized according to mantle length and expressed as $DML\,\mathrm{s^{-1}}$.

The time-averaged thrust, $\bar{F}_\mathrm{T}$, and lift, $\bar{F}_\mathrm{L}$, of a complete fin cycle (upstroke and downstroke) were calculated with the following equations:

$$\bar{F}_\mathrm{T} = \frac{I_{x\mathrm{U}} + I_{x\mathrm{D}}}{t_\mathrm{U} + t_\mathrm{D}} \tag{3}$$

$$\bar{F}_\mathrm{L} = \frac{I_{y\mathrm{U}} + I_{y\mathrm{D}}}{t_\mathrm{U} + t_\mathrm{D}}\ , \tag{4}$$

where $I_{x\mathrm{U}}$ is the horizontal component of the mean impulse produced by the upstroke, $I_{x\mathrm{D}}$ is the horizontal component of the mean impulse produced by the downstroke, t_U is the upstroke period, t_D is the downstroke period, and $I_{y\mathrm{U}}$ and $I_{y\mathrm{D}}$ are the vertical components of the mean impulse produced by the upstroke and downstroke, respectively. The magnitude and angular orientation of the time-averaged force produced by the complete fin cycle, $\bar{F}$, was geometrically calculated from thrust, $\bar{F}_\mathrm{T}$, and lift, $\bar{F}_\mathrm{L}$.

In many cases, vortices shed from sequential strokes were closely spaced or joined/merged. This prevented separate force estimates for upstrokes and downstrokes because of the potential interactions among neighboring vortices. For cases where groups of vortices were close together (within 1 ring diameter from one another) but widely separated from other vortices and boundaries (mode IV, Fig. 6F,G), the vortices were treated as a group with relevant hydrodynamic quantities computed as follows. Beginning with the general equation for hydrodynamic impulse, the impulse associated with a region of vorticity can be computed from:

$$\frac{\mathbf{I}}{\rho} = \frac{1}{2}\int \mathbf{x} \times \boldsymbol{\omega}\,\mathrm{d}V\ , \tag{5}$$

where $\boldsymbol{\omega}$ is the vorticity vector, $\mathbf{x}$ is the position vector, and $\mathbf{I}$ is the impulse vector (Saffman, 1992). For the case where the vortices are axisymmetric vortex rings that do not intersect, Eqn 5 reduces to:

$$\frac{\mathbf{I}}{\rho} = \sum_i \pi\,\hat{\mathbf{a}}_i \int_i \omega_\theta r_i^2\,\mathrm{d}r\,\mathrm{d}x\ , \tag{6}$$

where the sum is over all vortices, i, in the group, $\hat{\mathbf{a}}_i$ is a unit vector aligned with the axis of vortex i, and r_i is the radial distance from the axis of vortex i. That is, Eqn 1 can still be used to compute the contribution of individual vortices to the total impulse of the group of vortices as long as their orientation is properly accounted for and the results are combined vectorially to obtain the total hydrodynamic impulse $\mathbf{I}$. Using this observation, the axis of each vortex in the group was identified as the line midway between the vorticity peaks associated with each vortex ring in the group and orthogonal to the line connecting the peaks. Then the impulse associated with each vortex ring was computed using Eqn 1 and combined vectorially (assuming the vortex centers are in the same plane) to obtain the total hydrodynamic impulse (total for the combined upstroke and downstroke) as in Eqn 6. Using this result, the impulse magnitude, $I=|\mathbf{I}|$, and horizontal and vertical components, I_x and I_y, were determined geometrically. Impulse values were converted to time-averaged forces by averaging the I_x and I_y values over two to six sequential fin cycles and dividing by the average fin beat period during these cycles.

For cases where vortices were shed in a nearly continuous, closely-packed train (mode II, Fig. 6C; Fig. 7A,B), the vortices were too close together to be considered 'isolated' and could not be segregated into groups. In this case, the interaction of the vortices was handled explicitly. To approximate the vortex interaction effect, the impulse associated with the lead vortex ring in the train was computed as:

$$\frac{\mathbf{I}}{\rho} = \pi\hat{\mathbf{a}}\int\omega_\theta r^2\,\mathrm{d}r\,\mathrm{d}x - \sum_i\int_{t_i}\int\mathbf{u}_{e,i}\times\boldsymbol{\omega}\,\mathrm{d}V\mathrm{d}t$$

$$\approx \pi\hat{\mathbf{a}}\int\omega_\theta r^2\,\mathrm{d}r\,\mathrm{d}x - \sum_i\Delta t_i\int\mathbf{u}_{e,i}\times\boldsymbol{\omega}\,\mathrm{d}V\,, \qquad (7)$$

where $\hat{\mathbf{a}}$ is a unit vector aligned with the axis of the lead vortex, $\mathbf{u}_{e,i}$ is the velocity field induced on the lead vortex by trailing vortex i, Δt_i is the formation time of trailing vortex i (t_U or t_D as appropriate), and both spatial integrals are taken over the extent of the lead vortex (Saffman, 1992). For purposes of approximating the interaction integral (last term in Eqn 7), $\mathbf{u}_{e,i}$ was computed from the Biot-Savart induction law assuming the vorticity field of vortex i was axisymmetric about its own axis.

To use Eqn 7, the axis of each vortex involved in the calculation was determined in the same manner as the calculation involving Eqn 6. Then the interaction velocity $\mathbf{u}_{e,i}$ was determined for a specified number of vortices following the lead vortex in the train and the interaction integral is computed by integrating $\mathbf{u}_{e,i}\times\boldsymbol{\omega}$ over the lead vortex under the assumption that the lead vortex vorticity field was axisymmetric about its own axis. Unless otherwise specified, only one vortex following the lead vortex was used in the computation as the influence of more remote vortices on the lead vortex was minimal. Then, the terms in Eqn 7 were combined vectorially to find $\mathbf{I}$, where the impulse magnitude, $I=|\mathbf{I}|$, and horizontal and vertical components, I_x and I_y, were determined geometrically. Finally, to convert impulse values to time-averaged forces, the impulse $\mathbf{I}$ for leading vortices from two to six sequential fin cycles was computed from Eqn 7 and then the average I_x and I_y values were divided by the average fin beat period during these cycles.

Regardless of whether Eqns 6 or 7 was used to determine $\mathbf{I}$ and time-averaged forces for closely spaced vortices, the kinetic energy associated with the vortices in these situations was determined using:

$$\frac{E}{\rho} = \pi\int_{\mathrm{vortex}}\omega_\theta\psi\,\mathrm{d}r\,\mathrm{d}x\,, \qquad (8)$$

where ψ is the Stokes stream function. Eqn 8 assumes axisymmetry about the axis of the vortex ring. The stream function ψ was determined from the DPIV velocity field assuming axisymmetry about the axis of the vortex of interest. This assumption may not be valid – even if the vorticity field is axisymmetric – because of the influence of neighboring vortices. To reduce error in the calculation of ψ due to the effect of asymmetry in the velocity field, the integral in Eqn 8 was computed for both vortex cores (both positive and negative ω_θ) in each vortex ring and the results averaged together to determine the kinetic energy associated with a given vortex ring. The kinetic energy for an entire fin cycle is then obtained by summing the kinetic energy for the upstroke and downstroke vortices.

It should be noted that the current approach probably estimates the lower limits of fin force production. Because force was estimated from 2-D x–y cross sections of 3-D vorticity in the fin wake, lateral force components in the x–z plane were not included. Additionally, out-of-plane stretching or contraction of the vortices could not be captured.

Using the results for time-averaged thrust (determined from impulse using Eqns 1, 6 or 7 as appropriate) and vortex kinetic energy (from Eqn 2 or 8 as appropriate), fin propulsive efficiency was calculated for the various swimming speeds using the equation:

$$\eta_{\mathrm{P\,(fins)}} = \frac{\bar{F}_\mathrm{T}\bar{U}}{\bar{F}_\mathrm{T}\bar{U} + \bar{\dot{E}}_\mathrm{f}}\,, \qquad (9)$$

where $\eta_{\mathrm{P(fins)}}$ is the propulsive efficiency of the fins, $\bar{F}_\mathrm{T}$ is the time-averaged fin thrust, $\bar{U}$ is the mean swimming speed, and $\bar{\dot{E}}_\mathrm{f}$ is the time-averaged rate at which excess kinetic energy is shed by the fins, i.e. the peak excess kinetic energy measurement divided by the fin cycle period. Fin efficiencies were subsequently compared among fin modes. For swimming speeds where the fins produced net drag (negative thrust) over the fin cycle, an efficiency value of 0 was assigned.

RESULTS

Fin wake patterns

Hydrodynamic fin data from ten *Lolliguncula brevis* (3.7–6.2 cm *DML*) swimming tail-first at speeds from 0.19 to 1.89 $DML\,\mathrm{s}^{-1}$ and eight *L. brevis* (3.5–5.3 cm *DML*) swimming arms-first at speeds from 0.61 to 2.33 $DML\,\mathrm{s}^{-1}$ were analyzed. Vortices were present in some portion of the fin wake during all speeds for both orientations (Fig. 3B,C). As the fin began translating through a stroke, two regions of counter-rotating fluid developed near the leading and trailing edges of the fin, representing the upstream and downstream components of a single vortex, respectively. These regions of vorticity grew in strength through fin translation until stroke reversal, at which time the vortex was shed into the wake. Although 'leading-edge' and 'trailing-edge' are commonly used modifiers to describe the separate regions of vorticity shed from a fin, in the present study the orientation of the squid with respect to the flow may change (arms-first vs. tail-first swimming), so we choose to use the more general terms 'upstream vortex' and 'downstream vortex' to refer to leading-edge and trailing-edge vortices, respectively (Fig. 4). Typically the formation of the upstream and downstream vortices was synchronized, but during a few fin strokes the precise timing of vortex formation and subsequent shedding was not completely in phase.

Although vortices shed from a fin were consistently detected, fin wake signatures changed dramatically with swimming speed in terms of circulation strength, vortex size, vortex ring angle and interaction between separate vortex pairs. Each stroke (upstroke/downstroke) of a full fin beat cycle also exhibited different wake dynamics. All downstrokes produced vortices across the entire swimming speed range for both orientations, but some fin upstrokes were passive, i.e. no detectable vortices were shed, although most upstrokes did have associated vortices.

Four qualitatively distinct hydrodynamic fin wake patterns, referred to as swimming fin modes, were observed. Fin wake features such as vortex spacing, the presence/absence of vortices generated by fin strokes (upstrokes *versus* downstrokes), and the temporal pattern of vortex generation were used to qualitatively distinguish the different fin swimming modes. A schematic diagram of these modes is depicted in Fig. 5. In fin mode I (Fig. 6A,B), a single vortex was shed from the fin downstroke but the upstroke did not shed detectable vorticity into the wake. In fin mode II, denoted $\mathrm{II_T}$ for tail-first swimming (Fig. 6C) and $\mathrm{II_A}$ for arms-first swimming (Fig. 7A,B), a chain of seemingly linked vortices was produced by an undulating fin. In fin mode III, denoted $\mathrm{III_T}$ for tail-

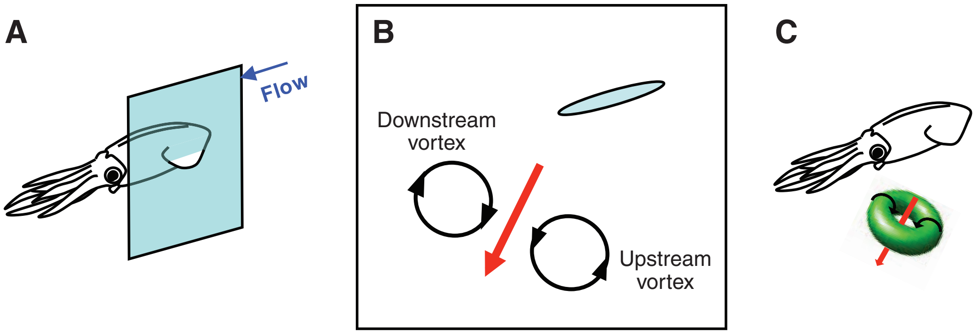

Fig. 4. Upstream and downstream components of a vortex shed from a fin of *Lolliguncula brevis*. (A) Diagram of the vertical *x*–*y* cross section of a squid fin. (B) The individual components of a vortex shed by a fin downstroke. The blue ellipse represents the position of the fin in the *x*–*y* cross section after completing a downstroke, and the red arrows indicate the central jet developed by the induced effect of the vortex ring. (C) Hypothetical 3-D vortex ring shed from the fin, including the upstream and downstream components as cross sections of the fully 3-D vortex.

first swimming (Fig. 6D,E) and III$_A$ for arms-first swimming (Fig. 7C,D), a fin cycle produced two separate vortices in the wake, one isolated vortex shed from the upstroke and one from the downstroke. Finally, in fin mode IV (Fig. 6F,G), each fin cycle shed a seemingly linked double vortex structure that was spatially separated from subsequent fin cycle vorticity. Although all four wake patterns were observed during tail-first swimming, only two (fin modes II$_A$ and III$_A$) were detected during the arms-first orientation. Selected variables from representative swimming sequences of each fin mode are included in Table 1.

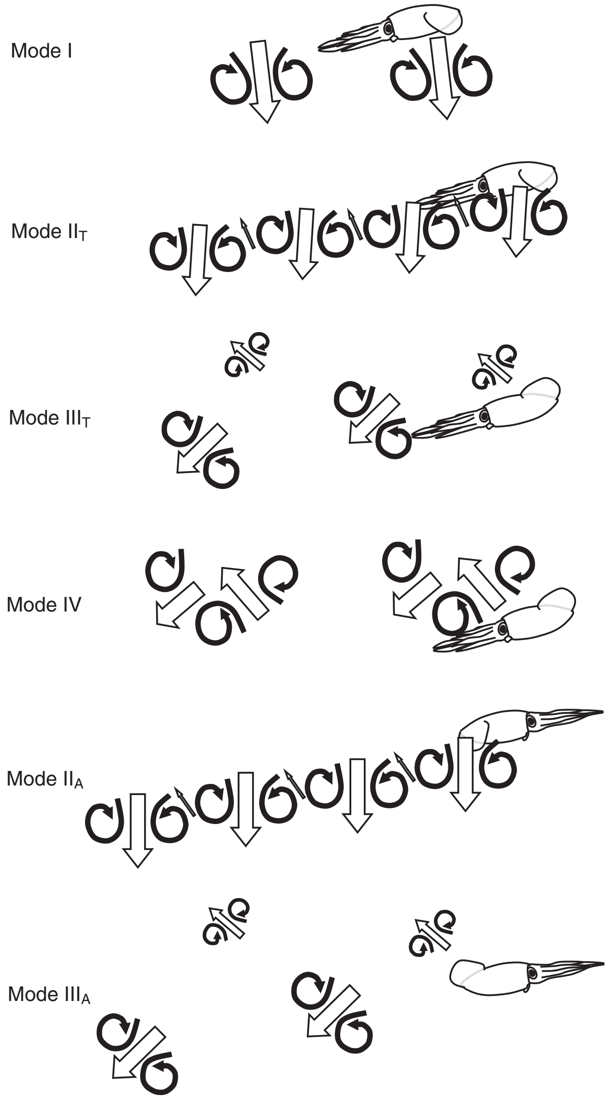

Fig. 5. Schematic 2-D fin wake signatures for *Lolliguncula brevis* presented for each swimming mode based on velocity vector fields and vorticity contours of the vertical *x*–*y* plane. Fin modes I, II$_T$, III$_T$, and IV represent tail-first swimming and fin modes II$_A$ and III$_A$ represent arms-first swimming. Curved arrows represent the vortex rotation with outlined arrows representing vortex central jets.

In fin mode I (Fig. 6A,B), which was only detected in tail-first swimming, the fin downstroke was a flapping motion that shed a single vortex into the wake while the preceding upstroke failed to generate detectable vorticity. For this mode, downstroke vortices of successive fin cycles were spaced greater than six vortex radii apart with presumably little vortex ring interaction. This mode was only observed at low velocities (0.19–0.54 $DML\,s^{-1}$) and was rare relative to other modes, occurring in only 12.5% of the swimming speeds tested (Fig. 8). The downstrokes shed vortices with average vortex ring angles exceeding 90 deg (β=104.7±8.80 deg, mean ± s.d., N=4), indicating a near vertical and slightly anterior fluid displacement.

The second swimming mode (fin mode II$_A$ and II$_T$) was detected in both swimming orientations (Fig. 7A,B, Fig. 6C). During this mode, the fin exhibited an undulatory motion, whereby more than one wavelength was present along the fin chord at any one time. Despite this undulation, during which there are no temporally distinct fin strokes as seen with the flapping motion, separate upstroke and downstroke vortices could be identified, based on the position of the fin's trailing edge upon vortex shedding. Each passing wavelength along the fin chord produced both an upstroke and downstroke vortex, which were spaced to allow the shed upstream vortex of each stroke to merge with the downstroke vortex of the next stroke in most cases. Owing to this close spatial arrangement and vortex generation pattern, vortices of sequential strokes appeared to be linked, producing a continuous chain of vorticity. Like fin mode I, this mode was rare for tail-first swimming, occurring in only 4% of the swimming speeds (Fig. 8) over a limited range (1.0–1.11 $DML\,s^{-1}$). The time-averaged force over a complete fin cycle was directed nearly downwards at an angle of 79.68±22.07 deg (N=4), indicating lift exceeded thrust.

The arms-first representation of the second swimming mode, fin mode II$_A$ (Fig. 7A,B), was the most common arms-first mode, occurring in 79% of the swimming speeds. As with the tail-first orientation (mode II$_T$), the fin exhibited an undulatory motion that produced a continuously linked chain of vortices in the wake. Again, the shed upstream vortex of the previous stroke served as the downstream vortex for the next stroke, resulting in significant interactions among vortices. This pattern was observed throughout the entire range of the recorded arms-first swimming speed (0.61–2.33 $DML\,s^{-1}$; Fig. 8). The downstroke vortices were generally

Table 1. Kinematic and force data from the fins of *Lolliguncula brevis* during six representative swimming sequences

Mantle length (cm)	Body mass (g)	Swimming speed (cm s^{-1})	Swimming orientation	Fin mode	Mean fin stroke period (s)	Mean fin stroke amplitude (cm)	Time-averaged thrust – two fins (mN)	Time-averaged lift – two fins (mN)
4.6	5.8	4.2	Tail-first	I	0.36 (*N*=5)	1.1 (*N*=5)	–0.29	2.0
4.6	5.8	5.1	Tail-first	II_T	0.48 (*N*=4)	1.2 (*N*=4)	0.29	1.6
3.7	4.6	4.2	Tail-first	III_T	0.40 (*N*=2)	0.74 (*N*=2)	0.37	0.78
5.3	10.8	6.0	Tail-first	IV	0.35 (*N*=5)	1.0 (*N*=5)	1.4	0.82
5.3	10.8	2.4	Arms-first	II_A	0.33 (*N*=3)	0.83 (*N*=3)	3.8	1.0
4.6	9.1	6.0	Arms-first	III_A	0.29 (*N*=3)	1.7 (*N*=3)	2.1	2.3

stronger (in terms of circulation) than the upstroke vortices. In fact, upstrokes, at times, shed very weak vorticity that immediately merged with the successive downstroke. As during tail-first swimming, the time-averaged force produced by a complete fin cycle was directed nearly downwards (β=83.10±17.36 deg; *N*=9) during arms-first swimming. In addition, there was no significant linear relationship between the angle in which the force was directed and the swimming speed (regression, r^2=0.012, *P*=0.775).

The third swimming mode (fin mode III_A and III_T) was also detected in both orientations (Fig. 7C,D, Fig. 6D,E). This mode was produced by a fin flap, whereby the fin wave was long relative to the fin chord and less than one full wavelength was present along the fin at all times. During tail-first swimming, fin mode III_T was more common than the two previously described tail-first modes (occurring in 25% of the swimming speeds) with a range of 0.37–1.66 *DML* s^{-1} (Fig. 8). Like fin mode II_T, fin mode III_T consisted of two shed vortices per fin cycle, an upstroke vortex followed by a downstroke vortex. However, the two vortices were more spatially and temporally separated from one another than in mode II_T, creating a chain of independent shed vortices with presumably little (or no)

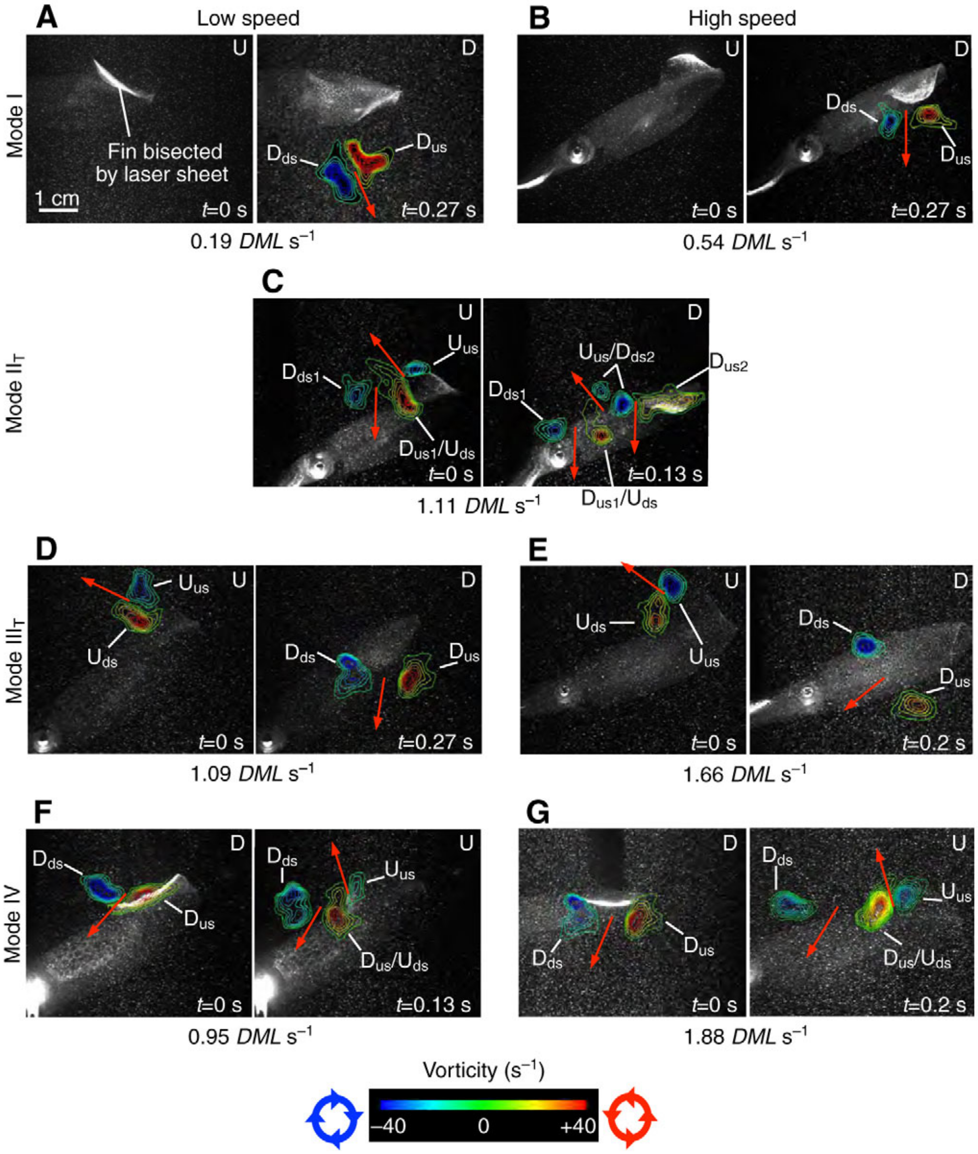

Fig. 6. Tail-first swimming fin wake signatures. (A–G) Vorticity contours illustrating the four unique fin swimming modes of *Lolliguncula brevis* in the tail-first orientation. Red regions represent counter-clockwise rotating flow and blue regions represent clockwise rotating flow. U_{ds}, upstroke downstream vortex, U_{us}, upstroke upstream vortex, D_{ds}, downstroke downstream vortex, and D_{us}, downstroke upstream vortex. Red arrows represent the central vortex jets and indicate their direction. (A,B) Fin mode I, (C) fin mode II_T, (D,E) III_T, and (F,G) fin mode IV. Aside from fin mode II_T, which was only detected at a narrow swimming speed range, each row contains two sets of image pairs, one pair collected during slower swimming and a second collected during faster swimming. The left image of a pair illustrates vorticity shed after the first stroke of a fin cycle and the right image illustrates vorticity shed after the second stroke. U, upstroke; D, downstroke.

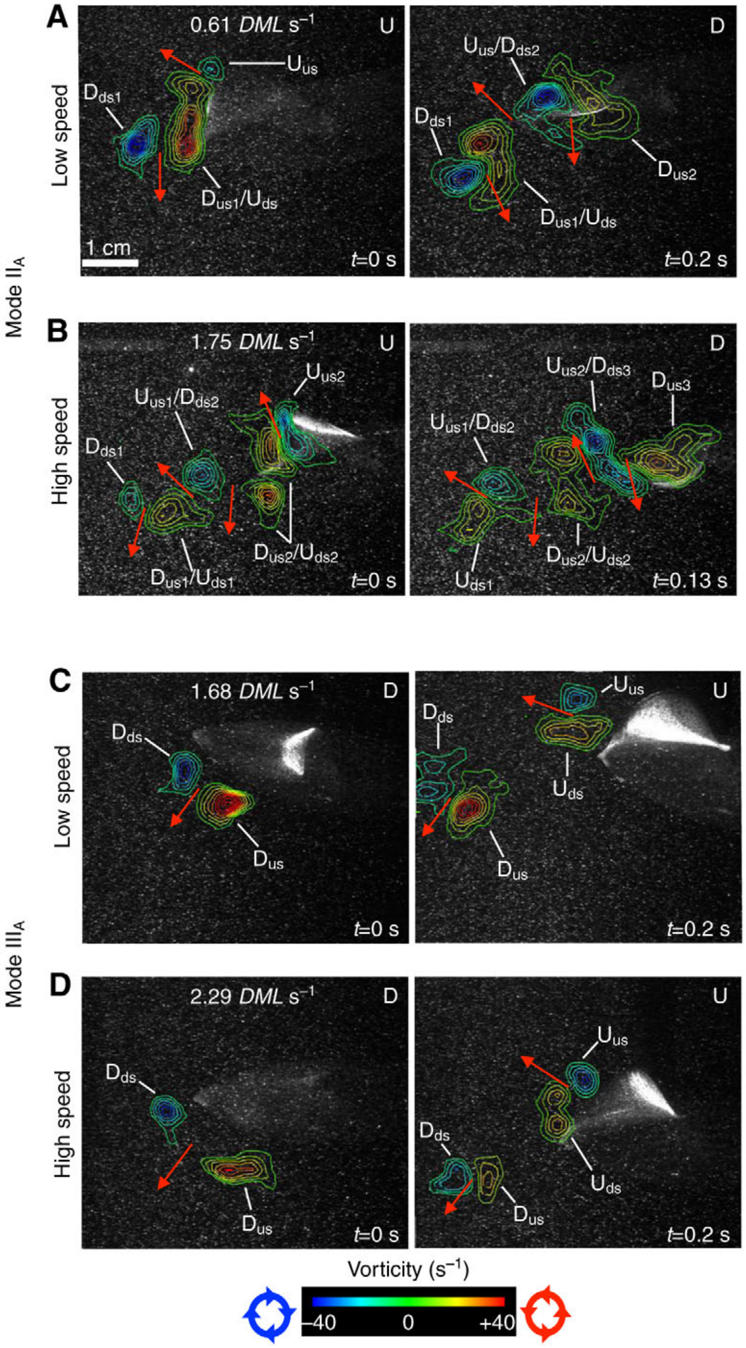

Fig. 7. Arms-first swimming fin wake signatures. (A–D) Vorticity contours illustrating the two unique fin swimming modes of *Lolliguncula brevis* in the arms-first orientation. Red regions represent counter-clockwise rotating fluid and blue regions represent clockwise rotating fluid. U_{ds}, upstroke downstream vortex; U_{us}, upstroke upstream vortex; D_{ds}, downstroke downstream vortex; and D_{us}, downstroke upstream vortex. Red arrows represent the central vortex jets and indicate their direction. (A,B) Image pairs illustrating fin mode II_A at slower and faster swimming speeds, respectively. (C,D) Image pairs illustrating fin mode III_A at slower and faster swimming speeds, respectively. The first image of a pair illustrates vorticity shed by the first stroke of a fin cycle and the second image illustrates the second stroke's shed vorticity. U, upstroke; D, downstroke.

interaction. Although both vortices of the fin cycle were prominent, the downstroke vortex was generally stronger in terms of circulation than the previous upstroke vortex. The average upstroke vortex ring angles varied across the speed range, from –28.3 to –78.8 deg, with a mean of –52.74±17.87 deg (N=6). Therefore, upstroke vortex rings were directed both upwards and counter to the direction of forward motion. The average downstroke vortex ring angles ranged from 39.9 to 79.6 deg, with a mean of 56.91±17.67 deg (N=6). Unlike the upstroke vortex ring angles, which showed no significant relationship with speed (regression, r^2=0.0075, P=0.8706), downstroke vortex ring angles decreased as swimming speed increased (regression, r^2=0.6956, P=0.039).

The arms-first representation of the third swimming mode, fin mode III_A (Fig. 7C,D), was observed in 31% of the arms-first swimming speeds. Like mode III_T, the fin exhibited a flapping motion that shed two isolated vortices per cycle, an upstroke vortex followed by a separate downstroke vortex. Again, these vortices were adequately spaced to presumably prevent linkage, producing a wake of isolated vortices alternating in upward and downward orientations. This mode was detected during higher swimming speeds (1.7–2.3 DML s^{-1}; Fig. 8). The upstroke and downstroke jet angles were both highly variable, with means of –29.1±18.2 deg (N=3) and 68.2±27.0 deg (N=3), respectively. The absolute values of the upstroke vortex ring angles were significantly less than the downstroke vortex ring angles (one-tailed paired t-test, d.f.=2, P=0.025), i.e. the fin upstrokes directed water more horizontally than the downstrokes. There were no significant linear relationships between the fin stroke vortex angles and the swimming speed

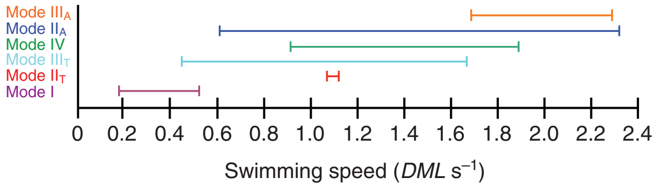

Fig. 8. Speed ranges of fin swimming modes for *Lolliguncula brevis*. Horizontal bars represent the swimming speed range in *DML* s^{-1} color coded for the respective swimming mode listed to the left. Modes I, $\mathrm{II_T}$, $\mathrm{III_T}$, and IV represent the tail-first swimming orientation and modes $\mathrm{II_A}$ and $\mathrm{III_A}$ represent the arms-first orientation.

(upstroke regression, r^2=0.157, *P*=0.741; downstroke regression, r^2=0.049, *P*=0.858).

The fourth swimming mode (fin mode IV; Fig. 6F,G) was only detected in tail-first swimming and was more frequently employed than all other tail-first modes combined, occurring in 54% of the swimming speeds. Like fin mode $\mathrm{III_T}$, the fin moved in a flapping motion with both upstrokes and downstrokes producing vortex rings. However, two isolated vortices were not produced for mode IV. Instead, the fin beat cycle began with a downstroke, which produced upstream and downstream vortices. After fin translation and downstroke vortex shedding, the fin immediately began the subsequent upstroke. The shed upstream vortex from the previous downstroke served as the downstream vortex for the upstroke, producing a seemingly linked double vortex system for each complete fin cycle. Unlike mode $\mathrm{II_T}$, however, each fin cycle's paired vortex structure was adequately separated from vorticity shed from subsequent cycles, producing a more discontinuous vortex chain. Fin mode IV only occurred at moderate to high speeds (0.92–1.89 *DML* s^{-1}; Fig. 8). The time-averaged force produced by complete fin cycles was directed posterioventrally at a mean angle of 48.5±21.9 deg (*N*=13). In addition, there was no a significant linear relationship between the angle in which the force was directed and the swimming speed (regression, r^2=0.0979, *P*=0.2979).

The propulsive efficiency of the fins ranged from 0 to 99.0% with a mean of 79.9±37.0% (*N*=24) during tail-first swimming. When fin propulsive efficiencies were compared among fin swimming modes, fin mode I was significantly less efficient than fin modes $\mathrm{II_T}$, $\mathrm{III_T}$, and IV (1-factor ANOVA, d.f.=23, $P<0.005$), whereas the mean propulsive efficiencies of fin modes $\mathrm{II_T}$, $\mathrm{III_T}$ and IV were statistically similar. During the arms-first orientation, the propulsive efficiency of the fins ranged from 0 to 98.9% with a mean of 57.2±48.8% (*N*=13). There was no significant difference in fin propulsive efficiency between fin modes $\mathrm{II_A}$ and $\mathrm{III_A}$ during the arms-first orientation (2 sample, 2 tailed *t*-test, d.f.=11, *P*=0.433).

Force estimates – tail-first swimming

Tail-first swimming modes were pooled to examine how fin force, fin force direction (force angle), fin thrust, and fin lift change with speed. Because upstroke and downstroke force estimates could not be hydrodynamically distinguished in fin modes $\mathrm{II_T}$ and $\mathrm{IV_T}$ due to vortex interactions, the time-averaged forces produced over the entire fin cycle (upstroke and downstroke) were analyzed for all swimming modes. Across the speed range, the time-averaged force produced by a single fin over the fin cycle ranged from 0.170 to 0.880 mN cm^{-2} and increased with swimming speed during the tail-first orientation (Fig. 9A; regression, r^2=0.585, $P<0.0001$). This time-averaged force was directed at angles (force angle) ranging from –6.26 to 113 deg. When analyzed over the speed range, force angle decreased with increasing swimming speed (Fig. 9B; regression, r^2=0.314, *P*=0.0037), i.e. the fins produced more horizontally oriented forces with increased speed. Fin thrust produced over the fin cycle ranged from –0.081 to 0.580 mN cm^{-2} (negative values

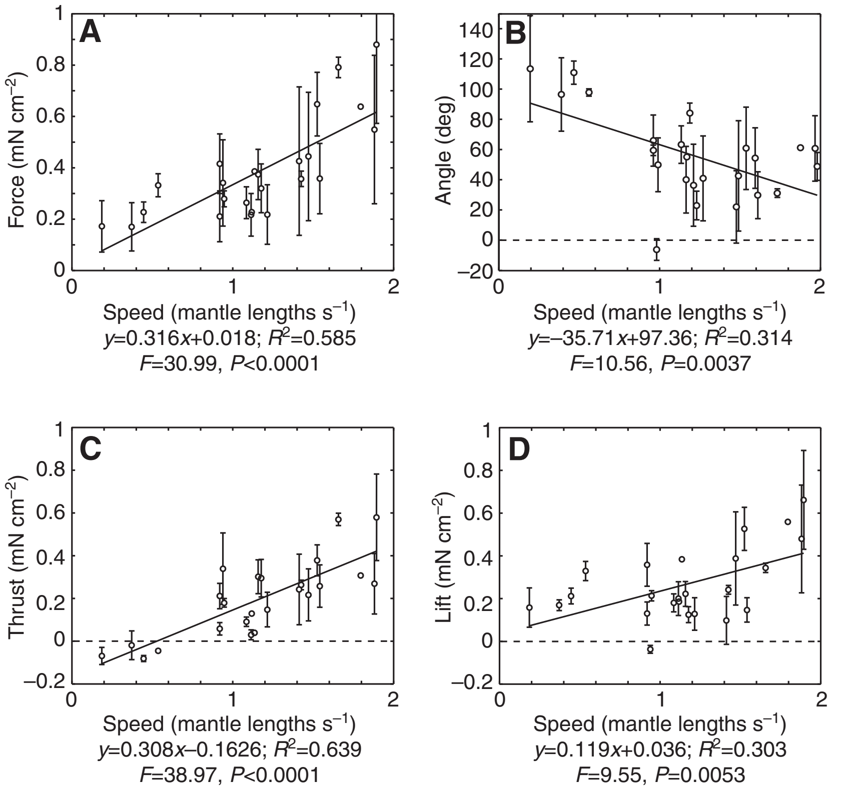

$y=0.316x+0.018$; $R^2=0.585$
$F=30.99$, $P<0.0001$

$y=-35.71x+97.36$; $R^2=0.314$
$F=10.56$, $P=0.0037$

$y=0.308x-0.1626$; $R^2=0.639$
$F=38.97$, $P<0.0001$

$y=0.119x+0.036$; $R^2=0.303$
$F=9.55$, $P=0.0053$

Fig. 9. Tail-first swimming force data. Force angles and magnitudes produced by a fin of *Lolliguncula brevis* during tail-first swimming. (A) The time-averaged force produced by a fin cycle as a function of swimming speed; (B) the angle in which the force was oriented. The total forces were geometrically decomposed into lift and thrust components: (C) the thrust produced by the fin cycle as a function of speed and (D) the corresponding lift. Any significant linear relationships include a best fit line and the regression equation, r^2 value, and *P* value are displayed below. All swimming velocities are reported as *DML* s^{-1} with forces normalized by fin area and reported as mN cm^{-2}. Error bars denote standard deviations of forces and force angles at each swimming speed.

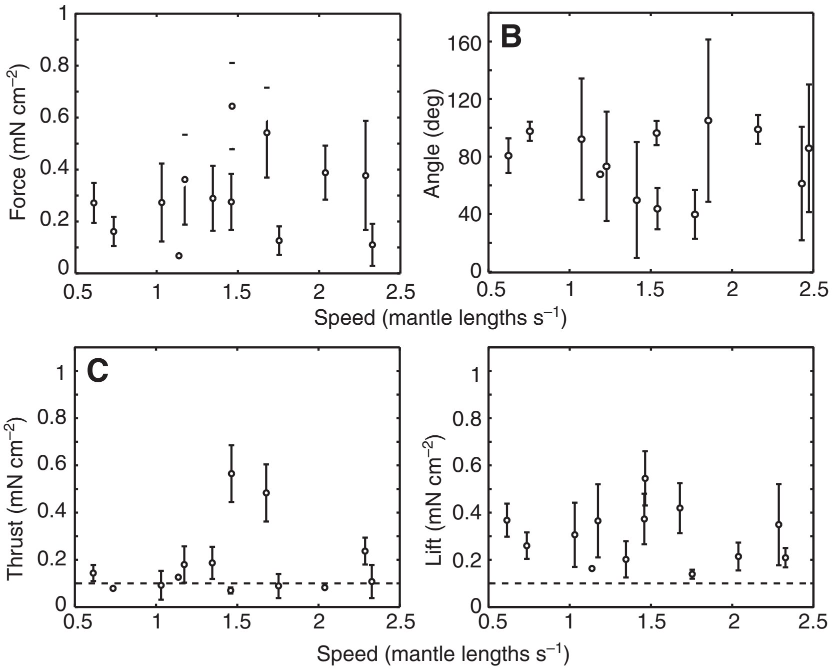

Fig. 10. Arms-first swimming force data. Force angles and magnitudes produced by a fin of *Lolliguncula brevis* during arms-first swimming. (A) The time-averaged force produced by a fin cycle as a function of swimming speed: (B) the angle in which the force was oriented. The total forces were geometrically decomposed into lift and thrust components: (C) the thrust produced by the fin cycle as a function of speed and (D) the corresponding lift. No significant linear relationships were detected for these data. All swimming velocities are reported as *DML* s^{-1} with forces normalized by fin area and reported as mN cm^{-2}. Error bars denote standard deviations of forces and force angles at each swimming speed.

reflect drag whereas positive values reflect thrust). In addition, fin thrust increased with increasing swimming speed (Fig. 9C; regression, r^2=0.639, P<0.0001). The fins produced lift values ranging from –0.037 to 0.662 mN cm^{-2} (negative values reflect forces pushing the animal downwards whereas positive values reflect forces pushing the animal upwards). Fin lift also increased with increasing swimming speed (Fig. 9D; regression, r^2=0.303, P=0.0053).

For fin mode III$_T$ a comparison between upstrokes and downstrokes was possible since sequentially shed vortices were adequately spaced. The time-averaged force produced during the fin upstrokes during fin mode III$_T$ ranged from 0.0310 to 0.353 mN cm^{-2} with a mean of 0.181±0.124 mN cm^{-2}, which was significantly less than the time-averaged force produced during the downstrokes (downstroke range=0.300–1.16 mN cm^{-2}, mean=0.539±0.324 mN cm^{-2}; paired-samples t-test, t=–3.61, d.f.=5, P=0.0154). The fin upstrokes produced thrust values ranging from 0.006 to 0.274 mN cm^{-2} with a mean of 0.120±0.098 mN cm^{-2}. The fin downstrokes produced thrust values ranging from 0.056 to 0.821 mN cm^{-2} with a mean of 0.323±0.282 mN cm^{-2} , which were not significantly different from those thrust values produced by the upstrokes (paired-samples t-test, t=–2.11, d.f.=5, P=0.0892). With regards to lift, the fin upstrokes produced negative lift ranging from –0.253 to –0.030 mN cm^{-2} with a mean of –0.129±0.0885 whereas the fin downstrokes produced positive lift ranging from 0.263 to 0.826 mN cm^{-2} with a mean of 0.413±0.212 mN cm^{-2}. When the absolute values of the lift contributions were compared, the downstrokes produced significantly greater lift forces than the upstrokes (paired-sample t-test, t=–4.41, d.f.=5, P=0.0069).

There were no significant differences in time-averaged force or lift production among fin modes I, II$_T$, III$_T$, and IV during tail-first swimming [1-factor ANOVA (force), d.f.=23, P=0.162; one-factor ANOVA (lift), d.f.=23, P=0.225)]. However, a significant difference in thrust production was detected among fin modes (1-factor ANOVA, d.f.=23, P=0.0036), with fin modes III$_T$ and IV producing significantly more thrust than fin mode I, while fin modes III$_T$ and IV were statistically similar.

Force estimates – arms-first swimming

The relationships of the time-averaged force produced over the entire fin cycle during arms-first swimming were different from those of tail-first swimming. During arms-first swimming, the time-averaged force produced by the fins ranged from 0.068 to 0.644 mN cm^{-2} with a mean of 0.299±0.167 mN cm^{-2}, and there was no significant linear relationship with swimming speed (Fig. 10A; regression, r^2=0.0185, P=0.656). The time-averaged force was directed in angles (force angle) ranging from 39.8 to 105 deg with a mean of 76.26±22.28 deg. In addition, force angle had no significant linear relationship with swimming speed (Fig. 10B; regression, r^2=0.0048, P=0.822). The time-averaged fin thrust produced over the fin cycle ranged from –0.030 to 0.465 mN cm^{-2} (negative values reflect drag whereas positive values reflect thrust) with a mean of 0.088±0.158 mN cm^{-2}, which was not significantly different from 0 (one-sample t-test, P=0.068). As with time-averaged force, there was no significant linear relationship of fin thrust with swimming speed during the arms-first orientation (Fig. 10C; regression, r^2=0.0151, P=0.698). Time-averaged lift produced over the fin cycle ranged from 0.039 to 0.445 mN cm^{-2} with a mean of 0.201±0.116 mN cm^{-2} and also there was no significant linear relationship with swimming speed during the arms-first orientation (Fig. 10D; regression, r^2=0.0185, P=0.658).

Since fin mode III also occurred during arms-first swimming, force contributions between upstrokes and downstrokes could be compared. Upstrokes generated time-averaged force values ranging from 0.00 to 0.2139 mN cm^{-2} with a mean of 0.119±0.0885 mN cm^{-2}, whereas downstrokes generated significantly greater time-averaged force values ranging from 0.501 to 1.29 mN cm^{-2} with a mean of 0.901±0.386 mN cm^{-2} (paired-samples t-test; t=–3.39, d.f.=3, P=0.0427). With regards to thrust, upstrokes generated thrust values ranging from 0.00 to 0.202 mN cm^{-2} with a mean of 0.103±0.0845 mN cm^{-2}. In comparison, downstrokes produced thrust values ranging from –0.119 to 0.931 mN cm^{-2} with a mean of 0.419±0.513 mN cm^{-2}, which were not significantly different from those values produced by upstrokes (paired-samples t-test, t=–1.13, d.f.=3, P=0.342). Upstrokes produced lift values ranging from –0.0995 to 0.00 mN cm^{-2} with a mean of –0.0527±0.0423 mN cm^{-2}

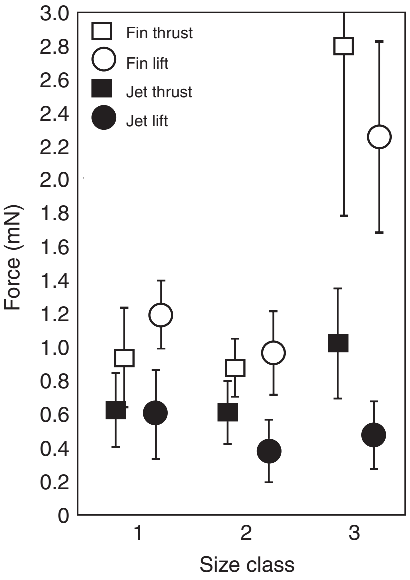

Fig. 11. Forces produced by both lateral fins and the jet of *Lolliguncula brevis* swimming between 1 and 2 *DML* s^{-1}. Black squares and circles represent jet thrust and lift, respectively, and white squares and circles represent fin thrust and lift, respectively. Jet force data courtesy of Bartol et al. (Bartol et al., 2009b). Size class 1: 4–4.9 cm *DML*, size class 2: 5–5.9 cm *DML*, size class 3: 6–6.9 cm *DML*. Error bars indicate ±1 s.e.m.

while downstrokes produced lift values ranging from 0.328 to 0.890 mN cm^{-2} with a mean of 0.646±0.281 mN cm^{-2}. When the absolute values of the lift contributions were compared, the downstrokes produced significantly greater lift forces than the upstrokes (paired-samples *t*-test, t=–5.78, d.f.=3, P=0.0103).

When fin force production was compared among fin swimming modes during the arms-first orientation, fin mode III$_A$ produced significantly more time-averaged force and thrust than mode II$_A$ [two sample one-tailed *t*-test (force), d.f.=11, P=0.0015;two sample one-tailed *t*-test (thrust), d.f.=11, P=0.0113], while lift production was similar among fin modes (two sample two-tailed *t*-test, d.f.=11, P=0.0952).

Arms-first *versus* tail-first force values

Arms-first and tail-first fin force contributions were also compared based on eight similar swimming speeds (±0.07 *DML* s^{-1}), ranging from 0.54 to 1.79 *DML* s^{-1}. For the speeds considered, the fins produced significantly more time-averaged force over the fin cycle during tail-first swimming than during arms-first swimming (one-tailed paired sample *t*-test, d.f.=7, P=0.031). When this force was geometrically decomposed into thrust and lift, the fins produced significantly more thrust during tail-first swimming (one-tailed paired sample *t*-test, d.f.=7, P=0.018) whereas there was no significant difference in lift production between orientations (two-tailed paired sample *t*-test, d.f.=7, P=0.19).

DISCUSSION

Although both the jet and fins are generally active during swimming, some previous locomotive studies on squid have largely ignored the fins as propulsors and focused primarily on the jet (Anderson and DeMont, 2000; Anderson and Grosenbaugh, 2005; Johnson et al., 1972; O'Dor, 1988). In the present study, vortex formation around fins was quantified using DPIV and fin force production was estimated from vorticity fields for the first time in any cephalopod. The results indicate that the fins of *Lolliguncula brevis* produce hydrodynamically relevant forces when compared to the pulsatile jet (Fig. 11), generating lift, thrust, and/or drag, in varying degrees, depending on swimming speed, and swimming orientation. During tail-first swimming, force data suggest the fins play an important role in stability at low swimming speeds, often producing drag, while shifting to greater thrust production as speed increases. Fin lift also increases with swimming speed during tail-first swimming. By contrast, arms-first force data suggest neither fin thrust nor lift is linearly dependent on swimming speed and lift is the fins' main responsibility. Moreover, *L. brevis* exhibited four qualitative fin wake patterns, or swimming modes, each with distinctive vortex ring structures, and overall demonstrated great versatility in locomotive fin function. Because the jet also produces locomotive forces, with the arms providing some additional lift, the fins generate only a portion of a squid's total thrust and lift. The variability in fin force production and diversity in wake patterns observed in this study together with results from Bartol et al. (Bartol et al., 2008) reflect the complex interplay among the different systems.

Although the current study provides the first global quantitative data from around squid fins, it is not the first study suggesting squid fins aid in locomotion. Zuev (Zuev, 1966) demonstrated that *Sthenoteuthis oualaniensis* and *Illex illecebrosus* achieve similar swimming velocities but have difficulty maintaining altitude and consistent trajectories when their fins are amputated, suggesting the fins provide not only stability, but lift as well. By contrast, Webber and O'Dor (Webber and O'Dor, 1986) and O'Dor and Webber (O'Dor and Webber, 1991) later reported that the fins of *Illex illecebrosus* provide negligible lift or thrust and function only in steering during the majority of swimming speeds, whereas the undulatory fin movements of *Doryteuthis opalescens* [formerly *Loligo opalescens* (see Vecchione et al., 2005)] augment locomotive forces only at very low speeds, when the fin waves travel faster than the animal's velocity. O'Dor (O'Dor, 1988) further investigated fin function and, at the lowest swimming speeds, estimated the fins provide up to 38% of the total thrust for *Doryteuthis opalescens* and 25% of the total thrust for *Illex illecebrosus*, but do not aid in propulsion during moderate to high speeds. Hoar et al. (Hoar et al., 1994) later explored squid fin diversity and predicted that, based on a heavy reliance on fin motion over a variety of swimming speeds, the fins of coastal squid are important propulsive contributors, providing supplemental thrust to the jet. Anderson and DeMont (Anderson and DeMont, 2005) studied kinematics of the squid *Doryteuthis pealeii* [formerly *Loligo pealeii* (see Vecchione et al., 2005)] and predicted the fins contribute a large portion of total thrust needed for movement. Bartol et al. (Bartol et al., 2001b) further emphasized the importance of fins and estimated high propulsive contributions based on force balance equations. For example, the fins of *Lolliguncula brevis* could potentially generate up to 83.8% of the total lift and 55.1% of the total thrust at low speeds. While these previous studies predicted fin force contributions based on kinematics and force balance equations, the current study provides more direct and quantitative measurements of force production using DPIV data of the fin wake.

When considering a squid's dual locomotive system, it is useful to consider propulsive efficiency. A squid's pulsatile jet is thought to be inherently less efficient than an undulating/oscillatory fin because of the volume limitations of the jet, although recent studies have indicated that pulsed jets can also be efficient at high speeds and/or when pulses are short (Anderson and Grosenbuagh, 2005; Bartol et al., 2008; Bartol et al., 2009a; Bartol et al., 2009b). Whereas a fin is less volumetrically restrained and can displace a large volume of water at low velocity, a jet often displaces a relatively small volume of water housed in a volumetrically limited mantle at a higher speed to achieve the same thrust, which may be energetically costly (Vogel, 1994). This inverse relationship between jet velocity and propulsive efficiency is reflected in the Froude efficiency equation:

$$\eta_\mathrm{P} = \frac{2U}{U_\mathrm{j} + U}\ , \tag{10}$$

where U is the swimming velocity and U_j is the jet velocity relative to the swimmer (Vogel, 2003). Given that fin recruitment presumably provides propulsive efficiency gains, it is not surprising that fin thrust was detected in the current study.

The propulsive benefits of fin activity for *L. brevis* are most significant for the speed range considered in this study. Bartol et al. (Bartol et al., 2008) reported the fins can increase overall locomotive efficiency by as much as 10.2% when active. Although *L. brevis* can swim at higher speeds than those examined in the current study, fin activity drops precipitously and ceases altogether at higher speeds (Bartol et al., 2001b). Given the presumed advantages of fin motion, why does fin activity decrease and ultimately cease as speed increases above the range explored here? Squid fins are tightly packed, three-dimensional muscular arrays known as ‘muscular hydrostats’ (Kier, 1988; Kier, 1989; Kier and Smith, 1985). Unlike the fins of fishes or the wings of birds, muscular hydrostats contain no hard supporting structures such as fin rays or bones, respectively. Instead, the tightly packed muscles provide both the force and support for movement (Kier, 1985). Although this arrangement allows for complex motions, the lack of skeletal support limits force production and prevents the attainment of high swimming speeds using fin propulsion alone (Kier, 1988; Kier, 1989; O’Dor and Webber, 1991). Consequently, the jet produces a greater proportion of the overall thrust as speed increases and fin force production declines (Bartol et al., 2001a; Bartol et al., 2001b; Bartol et al., 2008; O’Dor, 1988). When thrust production no longer exceeds drag because of structural limitations of the muscular hydrostatic system, *L. brevis* and other squids often wrap their fins around the mantle (Hoar et al., 1994; Bartol et al., 2001b) which provides a drag reduction benefit.

Fin wake patterns

In this study, four qualitatively distinct hydrodynamic fin wake signatures, or fin modes, were observed, two of which occurred during arms-first swimming and all four of which occurred during tail-first swimming. The reduced number of hydrodynamic wake signatures observed in arms-first swimming (fin modes $\mathrm{II_A}$ and $\mathrm{III_A}$) relative to tail-first swimming (fin modes I, $\mathrm{II_T}$, $\mathrm{III_T}$, and IV) may relate to differences in how the swimming orientations are employed ecologically. The arms-first orientation is used most extensively at low speeds when *L. brevis* is maneuvering in complex environments and investigating potential prey, whereas the tail-first orientation is used predominantly for sustained swimming (I.K.B., unpublished observation). Consequently, the constant flow characteristics of the water tunnel environment favor tail-first swimming, which was indeed the dominant orientation preference, and this fact alone may have contributed to the observance of more tail-first wake signatures. The more upstream location of the fins during tail-first swimming compared with arms-first swimming also leads to greater interaction of fin flows with the body, which could ultimately necessitate greater need for locomotive flexibility to enhance swimming efficiency (Weihs, 2002).

There are numerous references to animals with variable hydrodynamic signatures in the locomotive literature. In many animals, unique wake signatures are attributed to different locomotive ‘gaits’. For example, a bluegill sunfish’s pectoral fin sheds a single vortex during slow labriform swimming but produces two linked vortices at higher speeds (Drucker and Lauder, 1999). In addition, many birds exhibit a slow closed vortex gait during low speeds or hovering and a continuous vortex gait at high speeds (for details, see Alexander , 2002), with other intermediate wake patterns occurring as well (Spedding et al., 2003).

The concept of gaits has been applied successfully to terrestrial, aerial and aquatic locomotion. As speed increases, humans switch from walking to running, many birds switch from a closed to continuous vortex wake, and certain fish, such as *Lepomis*, switch from pectoral fin movements to body and caudal fin undulations (Alexander, 1989). No single locomotive style allows an animal to efficiently travel over a wide speed range. By employing different gaits, an animal varies its locomotion patterns to better match muscle power with locomotor power requirements (Alexander, 1989; Webb, 1993). The high density of water in relation to air, means that the thrust needed for aquatic propulsion increases much more rapidly with speed than the thrust needed for aerodynamic propulsion. Consequently, aquatic swimmers, in particular, must employ different gaits over their speed range (Webb, 2006). The four qualitatively unique fin wake patterns described in the present study could represent different locomotive gaits. Squids employing various fin gaits, even over the limited speed range investigated in the present study, can better meet swimming power requirements to increase efficiency (Webb, 1993). However, further study involving energetic measurements, electromyography, and/or more quantitative hydrodynamic metrics is necessary to determine if the fin wake patterns observed in the present study are indeed fundamentally distinct locomotive gaits.

The high number of fin wake patterns, or swimming modes, observed in the current study is probably attributable to the muscular hydrostatic system of the fins, whereby muscles are arranged in complex architectures, allowing for vast ranges of movement without support from bones or fluid cavities. Fin consist of three mutually perpendicular orientations of musculature: transverse, dorsoventral, and longitudinal fibers (Kier, 1989). Transverse fibers run horizontally from the base of the fin to the fin margin, dorsoventral fibers extend vertically from the fin’s ventral and dorsal surfaces, and longitudinal fibers lie horizontally, parallel to the fin chord. In addition, the transverse and dorsoventral muscle masses contain connective tissue fibers that potentially aid in support and provide elastic energy storage. To induce a fin movement, all three muscle fiber types simultaneously contract in different degrees to provide both the force and support for movement. Because of the squid’s sophisticated coordination of fin muscle contractions, the muscular hydrostatic system can generate a wide range of motions that ultimately produce complex wake patterns. In addition, the transverse muscles contain two types of fibers with contrasting aerobic capacities (Kier, 1989). The aerobic, mitochondria rich fibers most likely produce gentle undulations for low-speed swimming whereas the anaerobic glycolic fibers probably produce fin flapping at higher speeds (Kier, 1989; Kier et al., 1989). In addition, Johnsen and Kier (Johnsen and Kier, 1993) suggest that connective tissue fibers (as opposed to muscle fibers) provide passive muscular support during low amplitude/low frequency fin movements, potentially increasing fin efficiency at low speeds. According to these predictions, the undulatory fin movements responsible for fin mode II are likely to be driven primarily by aerobic muscle activity. However, future EMG studies that examine muscle activity in the two transverse fiber types are needed to corroborate this prediction.

Each of the four swimming modes has potential advantages for various swimming speeds and/or orientations. During slow swimming or hovering, a squid needs low thrust for forward movement but still requires significant lift to counteract negative buoyancy and maintain altitude. Fin mode I, which was detected at relatively low speeds (0.19–0.54 *DML* s^{-1}), involved hydrodynamically inactive fin upstrokes, which is beneficial since hydrodynamically active upstrokes often produce negative lift. The fin downstrokes of fin mode I generated forces directed both ventrally and slightly opposite to the direction of motion, thus producing significant lift and slight drag. Although this lift generation is important for depth maintenance at low speeds when overall dynamic lift is low (Bartol et al., 2001a), the drag produced could possibly create an antagonistic force relationship with the thrust producing jet, thus increasing stability (Hoar et al., 1994). Negatively buoyant fish tilt their body at a slight angle of attack at low swimming speeds, when trimming forces used for stability control diminish. This behavior, known as ‘tilting,’ increases body drag, requiring propulsors to generate larger forces that better match resistance and facilitate stability control (Webb, 1993). In squid, drag produced by the fins necessitates elevated thrust generation from the jet which can be used more effectively to correct self-imposed and external perturbations.

Fin mode II_T and II_A involved a seemingly linked vortex chain dominated by strong downstrokes producing ventrally directed forces, resulting in significant lift but minimal thrust production over fin cycles. This suggests the fins primarily generated lift while the jet presumably contributed the majority of thrust necessary for movement at speeds where this mode was employed. Because undulatory fin motion is required to produce the seemingly linked vortex chain in fin mode II, its higher occurrence in arms-first swimming in the present study is consistent with the findings of Bartol et al. (Bartol et al., 2001b), that there was greater undulatory fin motions in the arms-first mode than the tail-first mode. Moreover, the exclusive use of mode II_A for low speed arms-first swimming is consistent with previous studies that report highest reliance on undulatory fin motions at low speeds in *L. brevis* (see Bartol et al., 2001b; Hoar, 1995).

Fin modes III and IV produced time-averaged forces that were more horizontally directed than in fin modes I and II, resulting in greater overall thrust production. In addition, both of these modes exhibited active upstrokes that also produced thrust at the cost of inherent negative lift. Since both drag and lift forces increase quadratically with speed ($F_L \propto V^2$; $F_D \propto V^2$), modes that maximize thrust with each stroke rather than lift should be favored at intermediate and high speeds, which was generally the case with fin modes III and IV in the present study, i.e. modes III_T and IV_T were employed more frequently at higher speeds during tail-first swimming and mode III_A was employed more frequently at higher speeds during arms-first swimming. Although both modes were employed at some overlapping speeds during tail-first swimming, mode IV was generally used at higher speeds during tail-first swimming, which may relate to its linked vortex structure. In mode IV, the shed upstream vortex of the downstroke served as the subsequent downstream vortex of the upstroke, which could potentially accelerate upstroke vortex development and augment circulation, as is the case for insect wings (Birch and Dickinson, 2003). This circulation augmentation would lead to enhanced upstroke thrust production, which is advantageous for higher speeds.

Fin propulsive efficiency also helps explain the use of modes III and IV during higher speed swimming. In the tail-first orientation, swimming modes III_T and IV had significantly higher fin propulsive efficiencies than mode I. Since fin propulsive efficiency is based on thrust, this result is not surprising. In mode I, the fins often generated net drag while the animal swam at a certain speed, in which case fin propulsive efficiency was set to 0. In modes III_T and IV, the fin generated net thrust at all speeds, causing fin propulsion efficiencies to be much higher than in modes I and II_T. It should be noted, however, that these efficiency calculations do not incorporate the thrust contributions of the pulsatile jet and assume squid achieve various swimming speeds from fin movements alone. Consequently, the fin propulsive efficiencies reported in the present study probably overestimate the efficiency that would be achieved by fin locomotion alone, but they are nonetheless useful for relative comparisons of the different modes.

During tail-first swimming, the fin propulsive efficiencies of swimming mode III_T were not significantly different from those of mode IV. Therefore, in spite of the two qualitatively unique wake patterns, both swimming modes served statistically similar roles in forward propulsion. This could be because (1) there are only slight discrepancies in the fin thrust contributions and subsequent efficiencies of the two modes, and a larger sample size would be needed to separate any statistically significant variation, or (2) the unique wake patterns function similarly in thrust production, as the efficiency calculations suggest, but function differently in some other facet of locomotion, i.e. lift, stability, maneuverability, energetics or muscle mechanics. For example, modes III_T and IV could produce different magnitudes of stability-producing lateral forces, which were not considered in the current study, while maintaining similar thrust contributions. As stated above, the apparent vortex linkage of mode IV could enhance circulation development and subsequent thrust production (Birch and Dickinson, 2003), allowing a fin to generate a given thrust at a lower energetic cost in comparison to a non-linked wake. Clearly, further investigation is needed to determine why squid employ two qualitatively distinct swimming modes with seemingly similar propulsive efficiencies.

Fin force production

Tail-first swimming

Squid use the tail-first swimming orientation over a wider range of swimming speeds than arms-first swimming, from low speed cruising to escape jetting (Bartol et al., 2001b; O’Dor, 1988). Tail-first swimming is likely to be preferred for steady swimming because (1) there is minimal bending of the funnel, which avoids the volume flux limitations encountered during arms-first swimming when the funnel is significantly curved (Bartol et al., 2001b) and (2) the fins are at the leading edge of the body, which is more beneficial for stability than if they were located more posteriorly (Weihs, 2002). According to previous studies, the fins of *L. brevis* remain active at low to moderate tail-first swimming speeds, but this activity tends to decrease with higher speed before the fins eventually wrap around the mantle to reduce drag at the highest speeds (Bartol et al., 2001b; Hoar et al., 1994). To achieve high swimming speeds, Bartol et al. (Bartol et al., 2001b) predicted that mantle contraction amplitude and/or frequency increase to augment thrust since the propulsive role of the fins declines. In addition, Bartol et al. (Bartol et al., 2001b) reported that these negatively buoyant swimmers maintain altitude in both arms-first and tail-first modes by directing the pulsatile jet downwards, positioning the mantle and arms at high angles of attack, and employing fin activity.

During 88% of the tail-first swimming speeds, both the upstroke and downstroke of a fin cycle were hydrodynamically active, i.e. non-zero swimming forces were detected. When considering a squid’s negative buoyancy and concomitant lift requirements, an active upstroke may seem surprising because of its inherent negative lift production. However, an active upstroke allows for constant thrust production throughout the fin cycle, which is beneficial especially at high speeds when large thrust forces are required. In addition, the entire fin cycle produced a net lift during 96% of the tail-first swimming speeds, meaning the fin downstrokes generated sufficient lift to cancel out the negative lift produced by the respective upstrokes (see Fig. 9D). During fast forward flight, many birds exhibit a closed vortex gait, whereby a wake of linked vorticity is shed during both wing upstrokes and downstrokes. In contrast to the squid's upstroke, a bird's upstroke produces continuous lift during the closed vortex gait as a result of circulation that remains bound to the wing (Rayner, 1993). This disparity may relate to key differences in wing/fin morphology and lift requirements between birds and squids, which generate lift differently (wing flapping *versus* fin, jet, and arm coordination) and locomote in dissimilar media (air *versus* water).

In the squid *Doryteuthis pealeii,* Anderson and DeMont (Anderson and DeMont, 2005) predicted that both fin upstrokes and downstrokes produce thrust, with downstrokes generally producing the majority of thrust over the fin cycle, especially at higher speeds. By contrast, when fin thrust contributions were compared for mode $\mathrm{III_T}$ in the present study, downstrokes produced thrust values that were not significantly different from those produced by upstrokes. However, these data only reflect a single fin mode over a limited portion of the speed range of *L. brevis*, and further comprehensive thrust comparisons between fin strokes across a wider speed range are necessary for *L. brevis*. Thrust comparisons between upstrokes and downstrokes during modes I, $\mathrm{II_T}$, $\mathrm{II_A}$, and IV were not possible in the present study because of closely spaced, interacting vorticity shed from sequential strokes.

In the current study, the entire fin cycle produced thrust values that increased with swimming speed in the tail-first orientation. Bartol et al. (Bartol et al., 2001b) also predicted the fins of *L. brevis* contribute more thrust as swimming speed increases, over a similar range of speeds, although the jet produces disproportionately more thrust than the fins as speeds increase beyond the range investigated here (Bartol et al., 2001b; Bartol et al., 2008). As mentioned earlier, this complement to the jet, i.e. fin activity, increases overall propulsive efficiency within this intermediate range where the fins are active (Bartol et al., 2008).

Fin cycles also produced lift values that increased with swimming speed during the tail-first orientation. Although lift generation is important for negatively buoyant swimmers such as *L. brevis*, this positive correlation between lift and swimming speed is surprising. Since lift scales quadratically with velocity ($F_L \propto V^2$), active or powered lift expenditure should decrease with increased speed. One explanation may involve activity of the squid's pulsatile jet. Bartol et al. (Bartol et al., 2001b; Bartol et al., 2009b) found that, at low swimming speeds, the pulsatile jet provides significant lift by displacing fluid downwards, whereas, at higher speeds, *L. brevis* orients the jet more horizontally to maximize thrust production and propulsive efficiency while providing minimal lift. To compensate, the fins are potentially recruited to generate a larger proportion of the animal's required lift at high swimming speeds. While this explanation seems likely for a swimmer employing a dual locomotive system, further investigation of the relative contributions of the fins and the jet is needed for confirmation.

Fin drag production during low speed tail-first swimming may well be a mechanism to enhance stability. At low speeds, trimming forces in aquatic animals become poorly matched to those needed to correct disturbances (Webb, 1993; Webb, 2006). To compensate for reduced effectiveness of trimming forces at low speeds, some fishes flex their fins to increase effector area and drag (Bone et al., 1995), whereas others pitch to increase angle of attack of trim devices and hence lift (Ferry and Lauder, 1996; He and Wardle, 1986; Webb, 1993; Wilga and Lauder, 2000). The elevated drag of the fin downstroke coupled with high mantle and arm angles at low speeds (Bartol et al., 2001b) may serve a similar function. Several fish locomotion studies have reported pectoral fins functioning in non-thrust roles while swimming, providing stability benefits (Drucker and Lauder, 1999; Drucker and Lauder, 2000; Drucker and Lauder, 2002; Drucker and Lauder, 2003) (for a review, see Drucker et al., 2006). Therefore, tail-first fin downstrokes seemingly undergo a locomotive shift with increasing speed, from stabilizers at low speed cruising to propulsors at higher speeds, all while generating net lift.

Arm-first swimming

In comparison to tail-first swimming, squid use arms-first swimming over a more limited speed range, from hovering to only moderate swimming velocities, and prefer this orientation during complex maneuvering, antagonistic encounters, and prey investigation (Bartol, 1999). When in the arms-first orientation, squid have an expanded field of view unobstructed by the large mantle (Bartol, 1999), and can readily employ rapid prey strikes (Hanlon and Messenger, 1996). However, the funnel must undergo a 90 deg or more bend to eject water posteriorly in the arms-first orientation, which constricts the funnel and drastically limits the water volume flux of the jet and concomitant force production (Bartol et al., 2001b). Because of this reduced volume flux, Bartol et al. (Bartol et al., 2001b) predicted that the fins contribute more to thrust in the arms-first orientation than the tail-first orientation, although lift production is fairly similar in these two modes. Data from the present study do not completely support this prediction. Lift production was not statistically different for the two swimming orientations, but the fins actually produced significantly more thrust during tail-first swimming than arms-first swimming when similar swimming speeds were compared. This unexpected finding may relate to jet refilling. In the arms-first orientation water can enter the mantle cavity during refilling easier than in the tail-first orientation because it does not have to change direction. This could allow for more frequent jets and greater concomitant jet thrust, resulting in reduced fin thrust requirements during arms-first swimming. Although it was not possible to investigate relative fin and jet thrust contributions with our planar DPIV setup, future studies with a 3-D volumetric flow quantification system capable of simultaneously quantifying fin and jet flows could provide the data needed to address this hypothesis.

Fin cycles produced positive mean thrust and lift forces for the arms-first swimming speed range. Unlike tail-first swimming, however, the relationships of with swimming speed with the total force, lift and thrust produced by fin cycles in the arms-first orientation were not linear. This could relate to two factors: (1) there is a high level of variability in the data because of flexibility of the squid's dual locomotive system or (2) the fins occupy a specific locomotive role that stays fairly constant for the speed range considered in this study. During arms-first swimming, the arm and jet positioning are more variable than during tail-first swimming (I.K.B., unpublished data), and this could lead to accompanying variability in fin force production, making it difficult to detect consistent differences with speed. The detection of only two fin modes and high lift but low thrust production during arms-first swimming lend support for the second factor.

Several fin characteristics of arms-first swimming suggest that producing lift, rather than thrust, is the main locomotive responsibility of the fins in this orientation. First, the fin cycles produced positive net lift during all speeds of arms-first swimming

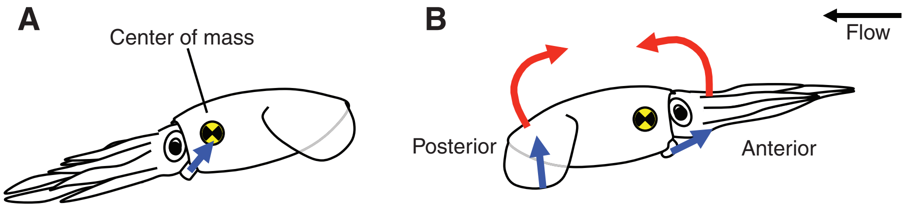

Fig. 12. Schematics illustrating the axis of the pulsatile jet in relation to a *Lolliguncula brevis'* center of mass during tail-first (A) and arms-first (B) swimming. Straight blue arrows indicate the resultant forces produced by the pulsatile jet and the fin whereas curved red arrows indicate resultant pitching moments. In A, notice the axis of the jet force passes close to the squid's center of mass. In B, the axis of the jet force is anterior to the center of mass, creating a positive pitching moment upstream of the head. Notice the near vertically oriented force generated by the fin produces a negative pitching moment that potentially balances the positive pitching moment of the jet.

(see Fig. 10D). In spite of hydrodynamically active fin upstrokes inherently producing negative lift during many speeds, a net lift was still achieved by strong downstrokes displacing fluid downwards at high angles. Second, the fins produced negative thrust (drag) more frequently in the arms-first orientation than in the tail-first orientation (the fins produced drag during 38% and 17% of the swimming speeds while in the arms-first and tail-first orientations, respectively). In fact, the fins produced no significant thrust when averaged over the speed range during arms-first swimming. Third, unlike tail-first swimming, fin thrust production did not increase with swimming speed in the arms-first orientation, suggesting the fins are not recruited for thrust production to achieve higher speeds.

Upwardly directed fin forces (lift) may be particularly important for stability in the arms-first orientation. During arms-first swimming, the pulsed jet is directed along an axis that is farther from the center of mass than during tail-first swimming, resulting in greater pitching moments (Fig. 12). For example, upwardly directed fin forces may produce moments posterior to the squid's center of mass (Fig. 12B). These moments can counter positive pitching moments created by the pulsed jet, which directs flow downward, rearward and anterior to the center of mass. Although the exact magnitudes of these pitching moments remain unknown, this pitch correcting system would be particularly advantageous over the low speed range investigated in the present study where stability control is most difficult (Webb, 2006).

Future directions

The two-dimensional flow quantification analysis presented in this study has several limitations. Two-dimensional force data relied on the axisymmetric assumption, treating each vortex pair as a symmetric ring. Although 2-D DPIV provides important information on wake dynamics, true 3-D flow analysis is necessary to more confidently distinguish between different swimming modes and to accurately reconstruct wake signatures. In the current study, 2-D DPIV data suggest that vortex merging occurs in modes II and IV, but only with true volumetric global flow visualization and quantification data will this be known for certain. New emerging technologies such as defocusing digital particle image velocimetry (DDPIV) that allow for true volumetric flow visualization and quantification are on the horizon and hold great promise for addressing such areas (Gharib et al., 2002; Pereira and Gharib, 2002; Pereira and Gharib, 2004; Kajitani and Dabiri, 2005; Pereira et al., 2006).

Conclusions

This study provides the first quantitative global data set on fin flows in actively swimming squids. Based on 2-D DPIV data, the fins generated both vertically and horizontally oriented forces of varying degrees depending on swimming speed and orientation. During tail-first swimming, the fins functioned as stabilizers at low speeds before shifting to thrust generators as speed increased, all while generating net lift. During arms-first swimming, the fins primarily provided lift, with thrust production being secondary. Four principal fin wake patterns were detected, each with a different vortex structure. This wake diversity indicates that the fins are versatile locomotive structures, capable of matching locomotive force production with swimming requirements. Many studies involving squid swimming dynamics have largely ignored the fins and focused primarily on the jet, but the current data suggest the fins actively contribute to locomotive force production and should be considered when estimating overall squid swimming performance and energetics, especially for long-distance migrators. With the advent of new volumetric flow quantification tools such as DDPIV, it may soon be possible to study coordination between the jet and fins of squids, which is necessary for an integrated, comprehensive understanding of squid swimming.

LIST OF SYMBOLS AND ABBREVIATIONS

$\hat{\mathbf{a}}_i$	unit vector aligned with the axis of vortex i
β	vortex ring angle
DDPIV	defocusing digital particle image velocimetry
DML	dorsal mantle length
DPIV	digital particle image velocimetry
E	excess kinetic energy
$\bar{\dot{E}}_\mathrm{f}$	time-averaged rate at which excess kinetic energy is shed
$\bar{F}$	time-averaged force
F_D	drag force
F_L	lift force
$\bar{F}_\mathrm{L}$	time-averaged lift
$\bar{F}_\mathrm{T}$	time-averaged thrust
I	hydrodynamic impulse magnitude
$\mathbf{I}$	total hydrodynamic impulse vector
I_x	horizontal component of impulse
I_y	vertical component of impulse
r	radial coordinate
t	fin stroke period
$\mathbf{u}$	velocity vector field
U	swimming speed
$\bar{U}$	mean swimming speed
U_j	jet velocity relative to the swimmer
V	speed
$\mathbf{x}$	position vector
Δt_i	formation time of trailing vortex i
η_P	propulsive efficiency
$\eta_\mathrm{P(fins)}$	fin propulsive efficiency
ρ	fluid density
ψ	Stokes stream function
$\boldsymbol{\omega}$	vorticity vector
ω_θ	azimuthal component of vorticity

ACKNOWLEDGEMENTS

We gratefully acknowledge field assistance from Nathan Bowman, Christopher Skaggs, and the Virginia Institute of Marine Science's Eastern Shore Laboratory.

We would also like to thank M. Vecchione and two anonymous reviewers for their helpful comments. This research was funded by the National Science Foundation (IOS 0446229 to I.K.B., P.S.K. and J.T.T.) and the Thomas F. Jeffress and Kate Miller Jeffress Memorial Trust (J-852 to I.K.B.).

REFERENCES

Alexander, D. E. (2002). *Nature's Flyers.* Baltimore: The Johns Hopkins University Press.

Alexander, R. M. (1989). Optimization and gaits in locomotion of vertebrates. *Phys. Rev.* **69**, 1199-1227.

Anderson, E. J. and DeMont, M. E. (2000). The mechanics of locomotion in the squid *Loligo pealei*: locomotory function and unsteady hydrodynamics of the jet and intramantle pressure. *J. Exp. Biol.* **203**, 2851-2863.

Anderson, E. J. and DeMont, M. E. (2005). The locomotory function of the fins in the squid *Loligo pealei. Mar. Fresh. Behav. Phys.* **38**, 169-189.

Anderson, E. J. and Grosenbaugh, M. A. (2005). Jet flow in steadily swimming adult squid. *J. Exp. Biol.* **208**, 1125-1146.

Bartol, I. K. (1999). *Distribution, Swimming Physiology, and Swimming Mechanics of Brief Squid,* Lolliguncula brevis. PhD. dissertation. The College of William and Mary, VA, USA, 214 pp.

Bartol, I. K., Mann, R. and Patterson, M. R. (2001a). Aerobic respiratory cost of swimming in the negatively buoyant brief squid *Lolliguncula brevis. J. Exp. Biol.* **204**, 3639-3653.

Bartol, I. K., Patterson, M. R. and Mann, R. (2001b). Swimming mechanics and behavior of the shallow-water brief squid *Lolliguncula brevis. J. Exp. Biol.* **204**, 3655-3682.

Bartol, I. K., Mann, R. and Vecchione, M. (2002). Distribution of the euryhaline squid *Lolliguncula brevis* in Chesapeake Bay: effects of selected abiotic factors. *Mar. Ecol. Prog. Ser.* **226**, 235-247.

Bartol, I. K., Krueger, P. S., Thompson, J. T. and Stewart, W. J. (2008). Swimming dynamics and propulsive efficiency of squids throughout ontogeny. *Integ. Comp. Biol.* **48**, 720-733.

Bartol, I. K., Krueger, P. S., Stewart, W. J. and Thompson, J. T. (2009a). Pulsed jet dynamics of squid hatchlings at intermediate Reynolds numbers. *J. Exp. Biol.* **212**, 1506-1518.

Bartol, I. K., Krueger, P. S., Stewart, W. J. and Thompson, J. T. (2009b). Hydrodynamics of pulsed jetting in juvenile and adult brief squid *Lolliguncula brevis*: evidence of multiple jet 'modes' and their implications for propulsive efficiency. *J. Exp. Biol.* **212**, 1889-1903.

Birch, J. M. and Dickinson, M. H. (2003). The influence of wingwake interactions on the production of aerodynamic forces in flapping flight. *J. Exp. Biol.* **206**, 2257-2272.

Bone, Q., Marshall, N. B. and Blaxter, J. H. S. (1995). *Biology of Fishes*. New York: Chapman and Hall.

Drucker, E. G. and Lauder, G. V. (1999). Locomotor forces on a swimming fish: three-dimensional vortex wake dynamics quantified using digital particle image velocimetry. *J. Exp. Biol.* **202**, 2393-2412.

Drucker, E. G. and Lauder, G. V. (2000). A hydrodynamic analysis of fish swimming speed: wake structure and locomotor force in slow and fast labriform swimmers. *J. Exp. Biol.* **203**, 2379-2393.

Drucker, E. G. and Lauder, G. V. (2001). Wake dynamics and fluid forces of turning maneuvers in sunfish. *J. Exp. Biol.* **204**, 431-442.

Drucker, E. G. and Lauder, G. V. (2002). Experimental hydrodynamics of fish locomotion: functional insights from wake visualization. *Integ. Comp. Biol.* **42**, 243-257.

Drucker, E. G. and Lauder, G. V. (2003). Function of pectoral fins in rainbow trout: behavioral repertoire and hydrodynamic forces. *J. Exp. Biol.* **206**, 813-826.

Drucker, E. G., Walker, J. A. and Westneat, M. W. (2006). Mechanics of pectoral fin swimming in fishes. In *Fish Biomechanics* (ed. R. E. Shadwick and G. V. Lauder), pp. 369-417. San Diego: Elsevier Academic Press.

Ferry, L. A. and Lauder, G. V. (1996). Heterocercal tail function in leopard sharks: a three dimensional kinematic analysis of two models. *J. Exp. Biol.* **199**, 2253-2268.

Gharib, M., Pereira, F., Dabiri, J., Hove, J. and Modarress, D. (2002). Quantitative flow visualization toward a comprehensive flow diagnostic tool. *Integ. Comp. Biol.* **42**, 964-970.

Hanlon, R. T. and Messenger, J. B. (1996). *Cephalopod Behaviour.* Cambridge: Cambridge University Press.

Hanlon, R. T., Hixon, R. F. and Hulet, W. H. (1983). Survival, growth, and behavior of the loliginid squid *Loligo plei, Loligo pealei,* and *Lolliguncula brevis* (Mollusca: Cephalopoda) in closed seawater systems. *Biol. Bull.* **165**, 637-685.

He, P. and Wardle, C. S. (1986). Tilting behavior of the Atlantic mackerel, *Scomber scombrus,* at low swimming speeds. *J. Fish Biol.* **29**, 223-232.

Hoar, J. A. (1995). *The Changing Role of Fins in Growing Loliginid Squid (Mollusca; Cepholopoda).* PhD dissertation, Dalhousie University, Halifax, Nova Scotia, 98 pp.

Hoar, J. A., Sim, E., Webber, D. M. and O'Dor, R. K. (1994). The role of fins in the competition between squid and fish. In *Mechanics and Physiology of Animal Swimming* (ed. L. Maddock, Q. Bone and J. M. V. Rayner), pp. 27-43. Cambridge: Cambridge University Press.

Johnsen, S. and Kier, W. M. (1993). Intramuscular crossed connective tissue fibres: skeletal support in the lateral fins of squid and cuttlefish (Mullusca: Cephalopoda). *J. Zool. Lond.* **231**, 311-338.

Johnson, W., Soden, P. D. and Trueman, E. R. (1972). A study in jet propulsion: an analysis of the motion of the squid, *Loligo vulgaris. J. Exp. Biol.* **56**, 155-165.

Kajitani, L. and Dabiri, D. (2005). A full three-dimensional characterization of defocusing digital particle image velocimetry. *Meas. Sci. Tech.* **16**, 790-804.

Kier, W. M. (1985) The musculature of squid arms and tentacles: ultrastructure evidence for functional differences. *J. Morph.* **185**, 223-239.

Kier, W. M. (1988). The arrangement and function of molluscan muscle. In *The Mollusca, Form and Function* (ed. E. R. Trueman, M. R. Clarke and K. M. Wilbur), pp. 211-252. New York: Academic Press.

Kier, W. M. (1989). The fin musculature in cuttlefish and squid (Mollusca, Cephalopoda): morphology and mechanics. *J. Zool. Lond.* **217**, 23-38.

Kier, W. M. and Smith, K. K. (1985). Tongues, tentacles and trunks: the biomechanics of movement in muscular hydrostats. *Zool. J. Linnean Soc.* **83**, 307-324.

Kier, W. M., Smith, K. K. and Miyan, J. A. (1989). Electromyography of the fin musculature of the cuttlefish *Sepia officinalis. J. Exp. Biol.* **143**, 17-41.

Messenger, J. B., Nixon, M. and Ryan, K. P. (1985). Magnesium chloride as an anaesthetic for cephalopods. *Comp. Biochem. Physiol. C Pharmacol. Toxicol. Endocrinol.* **82**, 203-205.

Müller, U. K., Van den Heuvel, B., Stamhuis, E. J. and Videler, J. J. (1997). Fish foot prints: morphology and energetics of the wake behind a continuously swimming mullet (*Chelon labrosus* Risso). *J. Exp. Biol.* **200**, 2893-2906.

Müller, U. K., Stamhuis, E. J. and Videler, J. J. (2000). Hydrodynamics of unsteady fish swimming and the effects of body size: comparing flow fields of fish larvae and adults. *J. Exp. Biol.* **203**, 193-206.

O'Dor, R. K. (1982). The respiratory metabolism and swimming performance of the squid, *Loligo opalescens. Can. J. Fish. Aquat. Sci.* **39**, 580-587.

O'Dor, R. K. (1988). The forces acting on swimming squid. *J. Exp. Biol.* **137**, 421-442.

O'Dor, R. K. and Webber, D. M. (1991). Invertebrate athletes: trade-offs between transport efficiency and power density in cephalopod evolution. *J. Exp. Biol.* **60**, 93-112.

Peng, J., Dabiri, J. O., Madden, P. G. and Lauder, G. V. (2007). Non-invasive measurement of instantaneous forces during aquatic locomotion: a case study of the bluegill sunfish pectoral fin. *J. Exp. Biol.* **210**, 685-698.

Pereira, F. and Gharib, M. (2002). Defocusing digital particle image velocimetry and the three-dimensional characterization of two-phase flows. *Meas. Sci. Technol.* **13**, 683-694.

Pereira, F. and Gharib, M. (2004). A method for three-dimensional particle sizing in two-phase flows. *Meas. Sci. Technol.* **15**, 2029-2038.

Pereira, F., Stüer, H., Graff, E. C. and Gharib, M. (2006). Two-frame 3d particle tracking. *Meas. Sci. Technol.* **17**, 1680-1692.

Rayner, J. M. V. (1993). On aerodynamics and the energetics of vertebrate flapping flight. *Cont. Math.* **141**, 351-400.

Saffman, P. G. (1992). *Vortex Dynamics*. Cambridge, UK: Cambridge University Press.

Spedding, G. R., Rosén, M. and Hedenström, A. (2003). A family of vortex wakes generated by a thrush nightingale in free flight in a wind tunnel over its entire natural range of flight speed. *J. Exp. Biol.* **206**, 2313-2344.

Tytell, E. D. (2004). The hydrodynamics of eel swimming. I. Wake structure. *J. Exp. Biol.* **207**, 1825-1841.

Vecchione, M., Young, R. E., Guerra, A., Lindsay, D. J., Clague, D. A., Bernhard, J. M., Sager, W. W., Gonzalez, A. F., Rocha, F. J. and Segonzac, M. (2001). Worldwide observations of remarkable deep-sea squids. *Science* **294**, 2505-2506.

Vecchione, M., Roper, C. E., Widder, E. A. and Frank, T. M. (2002). In situ observations on three species of large-finned deep-sea squids. *Bull. Mar. Sci.* **71**, 893-901.

Vecchione, M., Shea, E., Bussarawit, S., Anderson, F., Alexeyev, D., Lu, C. C., Okutani, T., Roeleveld, M., Chotiyaputta, C., Roper, C. et al. (2005). Systematic of Indo-West Pacific loliginids. *Phuket Mar. Biol. Cent. Res. Bull.* **66**, 23-26.

Vogel, S. (1994). *Life in Moving Fluids*, 2nd edn. Princeton, NJ: Princeton University Press.

Vogel, S. (2003). *Comparative Biomechanics.* Princeton, NJ: Princeton University Press.

Webb, P. W. (1993). Is tilting behaviour at low swimming speeds unique to negatively buoyant fish? Observations on steelhead trout, *Oncorhynchus mykiss*, and bluegill, *Lepomis macrochirus. J. Fish Biol.* **43**, 687-694.

Webb, P. W. (2006). Stability and maneuverability. In *Fish Biomechanics* (ed. R. E. Shadwick and G. V. Lauder), pp. 369-417. San Diego: Elsevier Academic Press.

Webber, D. M. and O'Dor, R. K. (1986). Monitoring the metabolic rate and activity of free-swimming squid with telemetered jet pressure. *J. Exp. Biol.* **126**, 205-224.

Weihs, D. (2002). Stability *versus* maneuverability in aquatic locomotion. *Int. Comp. Biol.* **42**, 127-134.

Wilga, C. D. and Lauder, G. V. (2000). Three-dimensional kinematics and wake structure of the pectoral fins during locomotion in leopard sharks, *Triakis semifasciata. J. Exp. Biol.* **203**, 2261-2278.

Willert, C. E. and Gharib, M. (1991). Digital particle image velocimetry. *Exp. Fluids.* **10**, 181-193.

Zuev, G. V. (1966). Characteristic features of the structure of cephalopod molluscs associated with controlled movements. Ekologo-Morfologicheskie Issledovaniya Nektonnykh Zhivotnykh. Kiev, Special Publication. (Canadian Fisheries and Marine Services Translation Series **1011**, 1968).